

Electrochemical pore etching in germanium

C. Fang, H. Föll *, J. Carstensen

Chair for General Materials Science, Faculty of Engineering, Christian-Albrechts-University of Kiel, Kaiserstr. 2, D-24143 Kiel, Germany

Received 29 November 2005; received in revised form 2 February 2006; accepted 18 February 2006

Abstract

Nucleation and growth of electrochemically etched pores in Germanium (Ge) was investigated for n- and p- type Ge single crystals with {100}, {110}, and {111} orientations and doping concentrations of $(10^{14}–10^{18})\text{ cm}^{-3}$. Various types of electrolytes, illumination conditions (front side, back side or none), and pre-treatments for optimizing nucleation were used. Several kinds of macropores could be obtained, mostly for the first time. In particular, pores could be obtained in p-type Ge samples. Pore geometries, morphologies, and growth peculiarities were found to be quite different from other semiconductors. Nucleation is generally difficult, the preferred growth direction is $\langle 100 \rangle$ or $\langle 111 \rangle$, stop planes are of {110} type, and there is always a strong electropolishing component compromising pore geometry and stability. Porous membranes have been produced showing electrocapillarity effects.

© 2006 Elsevier B.V. All rights reserved.

Keywords: Germanium; Semiconductor electrochemistry; Pore etching; Pore morphologies; Crystallographic dependence of pore formation

1. Introduction

Germanium, not silicon, was the first semiconductor employed to demonstrate the key properties of transistors in 1947 [1]. Much research into Ge followed, including extensive electrochemical investigations [2–4]. However, not only is the 0.66 eV band gap of Ge too small for large-scale microelectronic applications, but its oxide is chemically rather unstable in contrast to SiO_2 . Research into Ge therefore was almost abandoned as soon as solid-state electronics switched to Si. In recent years Ge enjoys a certain “come-back” as part of Si-based microelectronics, cf. [5] and therefore is attracting rapidly growing interest once more.

From a basic research point of view, Ge has some special properties that are of interest in the context of investigating electrochemical pore formation in semiconductors:

- (i) Ge has one of the highest dielectric constants ($\epsilon(\text{Ge}) = 16.2$) among the conventional semiconductors (for comparison: $\epsilon(\text{Si}) = 11.7$, $\epsilon(\text{GaAs}) = 12.9$, $\epsilon(\text{InP}) = 12.5$) and thus is an interesting material for, e.g., photonic crystal applications [6]. Photonic crystals of good quality have been produced by pore etching in other semiconductors (for a review see e.g. [7]).
- (ii) Ge shows “electrocapillarity” [2], i.e. its surface can be electrically switched from hydrophilic (probably H-terminated) to hydrophobic (probably OH terminated) simply by changing the applied potential [8]. If membranes or filters could be produced from Ge, this property might find interesting applications.
- (iii) Ge lacks a stable oxide and that has always been viewed as a disadvantage in the past. However, this makes Ge–C bond formation and thus functionalization of the Ge surface easier, and the group of Buriak [9,10] has successfully explored the functionalization of Ge surfaces in this context.
- (iv) Ge resembles the III–V semiconductors with respect to its unstable oxide (it dissolves in water), but like Si, and unlike the III–V’s, it is not polar. Since these two properties have a major influence on pore etching,

* Corresponding author. Tel.: +49 431 880 6175/6181; fax: +49 431 880 6178.

E-mail addresses: cf@tf.uni-kiel.de (C. Fang), hfoell@tf.uni-kiel.de (H. Föll), jcarst@tf.uni-kiel.de (J. Carstensen).

Ge is a kind of “in-between” case and thus of basic interest for a better understanding of the mechanisms behind pore etching in semiconductors.

The latter point is of particular interest in the quest for a better understanding of semiconductor electrochemistry, and we will compare the results obtained in Ge to what is known in other semiconductors throughout this paper. For ease of reading, these comparisons are mostly made without matter-of-course qualifiers like “mostly” or “on average”, and if no special reference is given, we always refer implicitly to pore properties outlined in the review [11] for III–V semiconductors, or in the reviews [12–14] for Si and the references therein; alternatively the monographs of Lehmann [15] and Zhang [16] or the proceedings of the biannual conference on Porous Semiconductors Science and Technology (PSST) [17,18] might be consulted.

While by now there is a wealth of data for porous Si, very little work has been done on pore etching in Ge and until recently no “good” pores have been produced [19]. In consequence, before the work presented here was started, very little was known about the mechanisms of pore formation or anodization of Ge in acid [20] or in alkali solution [21]. Most of the published articles refer to optical properties of “porous” Ge (including porous layers obtained by “stain-etching”) [22–26], and little is said about the morphology of the porous layers.

For example, the Buriak group only obtained pores in n-type Ge samples by using a special method that required switching between anodic and cathodic conditions, while pores obtained by a direct anodic method were reported in [19]. More recently, Flamand et al. [27] presented a detailed attempt to produce microporous Ge layers, intended to be used for a lift-off technique similar to the ones demonstrated previously in porous Si [28]. While this endeavor was not yet successful, it showed once more that pore nucleation and growth in Ge is not as easy as in other semiconductors and underlined the necessity for more basic studies. Finally, Kelly et al. reported a 3D structure of macropores in Ge [6], but this structure was obtained by depositing Ge in a porous template [6] and not by etching.

The present paper attempts to present all the results obtained so far (including the preliminary results already published in short communications [19]) in a structured manner and to compare the salient features to those of other porous semiconductors. However, large parts of the available parameter space have not been explored so far, and new discoveries must be expected in the future.

2. Experimental

Most Ge samples were of n-type with low ($n = 10^{14}$ – 10^{15} cm^{-3}), moderate ($n = 10^{16}$ – 10^{17} cm^{-3}) or high doping ($n = 10^{18} \text{ cm}^{-3}$), polished or unpolished surfaces, and areas of typically 0.2 cm^2 ; some samples, however, were of p-type. Etching was performed in an electrochemical double cell with a four-electrode system, which is described in

detail in [29]. Essentially, the back side contact is formed by a (light-transparent) electrolyte, with the Ge-electrolyte contact being “open”, i.e. biased in forward direction. While this arrangement serves as a good ohmic contact in most applications, some care must be taken at low potentials; for more details consult [29].

The orientation of the samples was mostly {100}, but some experiments were also done with {110} and {111} samples. Some low-doped samples were relatively thick (1 mm), whereas the other samples usually had a thickness of about 300–500 μm . Samples were from different suppliers and may have had different levels of defect densities and surface perfection; however, all samples were of “semiconductor grade”, i.e. extremely pure and with small if not vanishing dislocation densities. For some experiments, the surface was abraded by a 3 μm DP-suspension SiC powder (diamond product) to investigate the effect of surface damage to pore nucleation.

The holes necessary for dissolution of n-type Ge were supplied either by electrical breakdown (most likely avalanche breakdown of the space charge region), and/or by front side or back side illumination (fsi and bsi, respectively). The most commonly used electrolyte was 5% HCl (always weight %) either obtained by diluting 37% HCl with water, or alternatively with dimethylsulfoxide (DMSO). The latter electrolyte was chosen in order to minimize the water content of the solution and thus possibly the kinetics of oxide formation or the “oxidation power” [14], and/or its GeO_2 dissolving capability. “Organic electrolytes” of this type allowed a whole range of new pore types in Si [30–33], and are thus of interest for Ge, too. On the other hand, in order to increase the “oxidation power” of the electrolyte (which also proved to be useful in Si [33]), some experiments have been conducted in H_2SO_4 , or $\text{HCl} + \text{CrO}_3$ containing electrolytes. In spite of the fact that the nucleation in this case was mostly very bad and resulted in big porous domains, the results for these electrolytes were generally consistent with the “current burst model” made for Si [14,34,35] that in more oxidizing electrolytes the diameter of pores should increase.

Considering that anions adsorb on Ge in the order: $\text{I}^- > \text{Br}^- > \text{Cl}^- > \text{F}^- > \text{SO}_4^{2-}$ [36], and that the correspondingly increased charge distribution across the inner Helmholtz layer appears to reduce the energy required for the anodic dissolution process, some experiments were performed with HF, H_2SO_4 and HBr based electrolytes, too; Fig. 1 shows typical results.

While pores could be produced in all cases under optimized conditions, HCl based electrolytes performed best, and in what follows we will mostly discuss this type of electrolyte.

All experiments were performed at constant temperature (controlled with an accuracy of typically $\pm 0.1 \text{ }^\circ\text{C}$), under potentiostatic or galvanostatic condition (controlled by a custom-built potentiostat/galvanostat) using a Pt pseudo-reference electrode (when indicated in what follows) or an Ag/AgCl reference electrode (when without indication

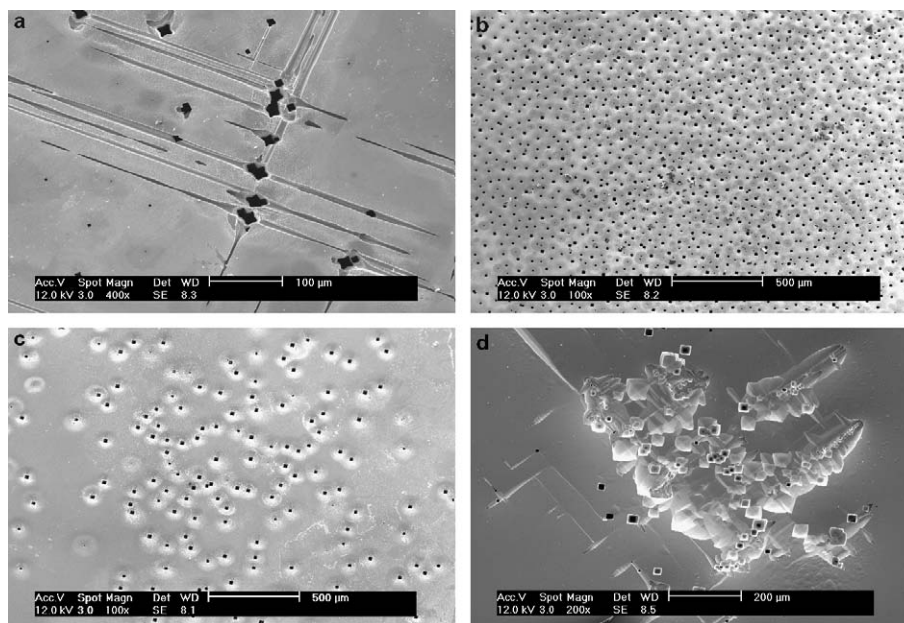


Fig. 1. “Typical” pores obtained with different unfavorable electrolytes under optimized conditions (see below). All samples are n-type in the dark, medium doping level, (100) oriented, polished surface, $T = 20\text{ }^{\circ}\text{C}$. (a) 5% HF aqueous electrolyte, ramp current from 0 to 5 mA/cm^2 in 60 min. Strong electropolishing, very inhomogeneous nucleation, strong side pores even under the surface in the bulk. (b) 5% HBr aqueous electrolyte, 5 mA/cm^2 for 60 min. Very large pores at low, uniform density. (c) 5% H_2SO_4 aqueous electrolyte, 5 mA/cm^2 for 60 min. Very large pores, not uniform, often some deposits in the pores. (d) 5% HCl + 1% CrO_3 aqueous electrolyte, ramp current from 0 to 10 mA/cm^2 in 60 min. Serious electropolishing takes place; growing pores is difficult.

in the text). The electrolyte was pumped through the cell at all times in order to optimize the transport of ions or molecules to and from the reactive interface. The etching time was typically 15–600 min.

The samples were investigated with a Philips XL series scanning electron microscope (SEM) in plain view and in cross-section after cleaving; on occasion the EDX spectrometer of the instrument was used. It is important to note that the cleavage plane is not always well-defined and not always $\{110\}$ as one would expect from cleaving solid Ge. However, all micrographs shown assume $\{110\}$ -cleavage plane if not otherwise noted.

The results obtained depend on the following factors, often in sensitive and unexpected ways: surface orientation, doping type and doping level, surface conditions (polished, “rough”, patterned), illumination (together with the minority carrier life time), electrolyte, temperature and etching conditions (galvanostatic, potentiostatic, ramped or “pulsed” conditions). It is thus difficult to develop a step-by-step picture of pore etching in Ge.

The format chosen to describe the results moves from more general to more special observations, and from areas in parameter space where many experiments have been performed to less frequently visited regions.

3. Results

3.1. Some general observations

Compared with other semiconductors, pore etching in Ge shows many new effects, some of which can be partially

understood in retrospect (see Section 4), but were mostly unexpected at the outset of the experiments. First, some of these observations will be listed in the context of comparable findings in other semiconductors; this will be helpful in understanding the more detailed results presented later and the design of certain experiments.

Only macropores have been obtained until now (meaning, by IUPAC standard, that pore diameters d_p are $>50\text{ nm}$). In particular, no micropores ($d_p < 10\text{ nm}$) or mesopores ($10\text{ nm} < d_p < 50\text{ nm}$) have been observed in this work; this again is more reminiscent of III–V’s than of Si. In the limited previous work, pores had only been obtained in n-doped Ge; macropores in p-type Ge are reported for the first time in this paper.

The doping level (or the directly related resistivity) usually defines two important length scales for pore etching in semiconductors: First the width of the space charge region (SCR), and second the radius of curvature necessary for a pore tip to induce avalanche breakdown at a given voltage, cf. e.g. [15] for Si data. In all other semiconductors these two length scales are usually rather directly expressed in the pore geometry, but not in Ge. So far, few observations can be tied to the doping level of Ge in an unambiguous way.

Another unexpected result, observed during the anodization of all types of Ge samples, is the general presence of some noticeable dissolution on all surfaces, even during stable growth of pronounced macropores. This means that current does not just flow almost exclusively at the pore tips, but that an appreciable amount flows through the side walls of the pores as well as through the sample surface

between pores. This will be referred to as “electropolishing”, but this term is not meant to imply that the corresponding dissolution reactions are perfectly isotropic. Due to electropolishing, the thickness of the sample decreases appreciably during etching, and plain view micrographs do not show the original surface as (approximately) in the case of pore etching in Si or III–V’s, but a cut through the structure at a depth that depends on the total etching time. Concurrently, pores may grow laterally, increasing their cross-sectional area and leading to conical over-all shapes.

Pore nucleation in Ge tends to be rather difficult, frequently causing very inhomogeneous pore distributions. This is somewhat reminiscent of GaAs or GaP; while Si, under most (but not all [37]) experimental circumstances, nucleates pores of all kinds rather uniformly without apparent problems. The surface conditions, but also many other factors, are very important for initial pore nucleation. Pore nucleation and subsequent pore growth proceed quite differently on polished, rough, or mechanically damaged surfaces; this will be treated in some detail.

The crystallography of pores in Ge is also quite different to those in other cubic semiconductors; it is more complicated and not yet fully understood. Generally, pores in semiconductors are either “crystallographic pores”, meaning that they grow in certain crystallographic directions independent of the surface orientation or of the electrical field direction, or they are “current line pores”, meaning that the pore direction coincides with the direction of current flow (or, same thing, the direction of the electrical field vector). Current line or “curro” pores thus usually grow perpendicular to the surface, for noteworthy exceptions in InP see [11,38]. Crystallographic or “crysto” pores often exhibit prismatic shapes or cross-sections exposing so-called “stop-planes”, i.e. the planes most resistant to (anisotropic) anodic dissolution. Crystallographic pores in Si always follow $\langle 100 \rangle$ directions, or (less pronounced) $\langle 113 \rangle$ directions, and stop planes are of the $\{111\}$ type. In III–V’s, crystallographic pores propagate along $\langle 111 \rangle_{\text{B}}$ directions (B meaning the $[111]$ direction pointing from the group V to the nearest group III element; here the polar nature of the III–V’s expresses itself), and stopping planes are of the $\{112\}$ type. In Si, InP and GaP, current-line pores have also been found (not yet in GaAs, though); in InP they provide for rather spectacular structures [11,39–41].

Ge is different: Crystallographic pores in $\langle 100 \rangle$ directions with well-defined prismatic shape definitely exist, but also in $\langle 111 \rangle$ directions. Strongly expressed stopping planes are of the $\{110\}$ type; but other planes, in particular $\{100\}$, are also frequently observed. Clear current line pores have not been observed so far, but that must not be seen as a proof of their general non-existence.

The current–voltage characteristic of n-Ge, while following the typical semiconductor behavior in general, has pronounced idiosyncrasies, too. In marked contrast to Si, and somewhat reminiscent of III–V’s (particularly GaAs),

some kind of breakdown occurs in most electrolytes at external voltages of just a few volts – even for samples with high resistivities and polished surfaces. While this behavior is generally reminiscent of junction breakdown at high field strength, the voltages observed are far lower than in comparable Si cases and do not scale with doping in the expected way.

Illumination of both types (front side illumination (fsi) or back side illumination (bsi)) will superimpose a substantial photocurrent, which will be noticeable in the voltage regime before breakdown occurs. The magnitude of the photocurrent for the bsi case depends strongly on the minority carrier diffusion length of the sample, and Ge is the only other semiconductor besides Si where the diffusion length is large enough to allow meaningful back side illumination experiments. The “bsi mode” was essential for macropore etching in n-type Si (its discovery actually triggered macropore research in Si [42]), but cannot be employed in other semiconductors, which have typically small diffusion lengths either because of a direct band gap (e.g. GaAs, InP) or because of lattice imperfection (e.g. GaP, SiC). It is thus of particular interest to employ bsi etching conditions in a semiconductor other than Si. The results obtained with Ge, however, so far are quite different from what is known from Si and not yet fully understood.

Another rather unique finding are pores filled with germaniumoxide, GeO_2 , which can be obtained under certain circumstances. While small remnants of SiO_2 have been found on occasion in pores in Si [43], nothing like the structures observed here was observed with other semiconductors.

Anodic dissolution of semiconductors often leads to self-ordering phenomena – from current or voltage oscillations in time, to current oscillations in space (i.e. ordered pore arrays) and combinations of the two, and many kinds of structure formation phenomena have been observed, cf., e.g. [14,44–46]. Ge, again, seems to be different. Pronounced voltage oscillations (and occasionally current oscillations) were frequently observed during pore growth, but no other self-induced ordering phenomena could be found up to now.

3.2. N-type $\{100\}$ samples in aqueous electrolytes

3.2.1. Current–voltage characteristics and influence of doping

The current–voltage (*IV*) characteristics of n-doped Ge samples under anodic bias are quite different from those of Si and not fully understood at present; Fig. 2 shows some examples. As a general feature, the Ge–electrolyte contact shows some of the expected behavior of a reversely biased diode that is susceptible to front- or back side illumination, but the details are often somewhat puzzling. In what follows, we will use the term “standard etching conditions” for the following set of variables: n-type, $\langle 100 \rangle$ orientation, polished surface, 20 °C, 5% HCl aqueous electrolyte, 120 min etching time, no illumination.

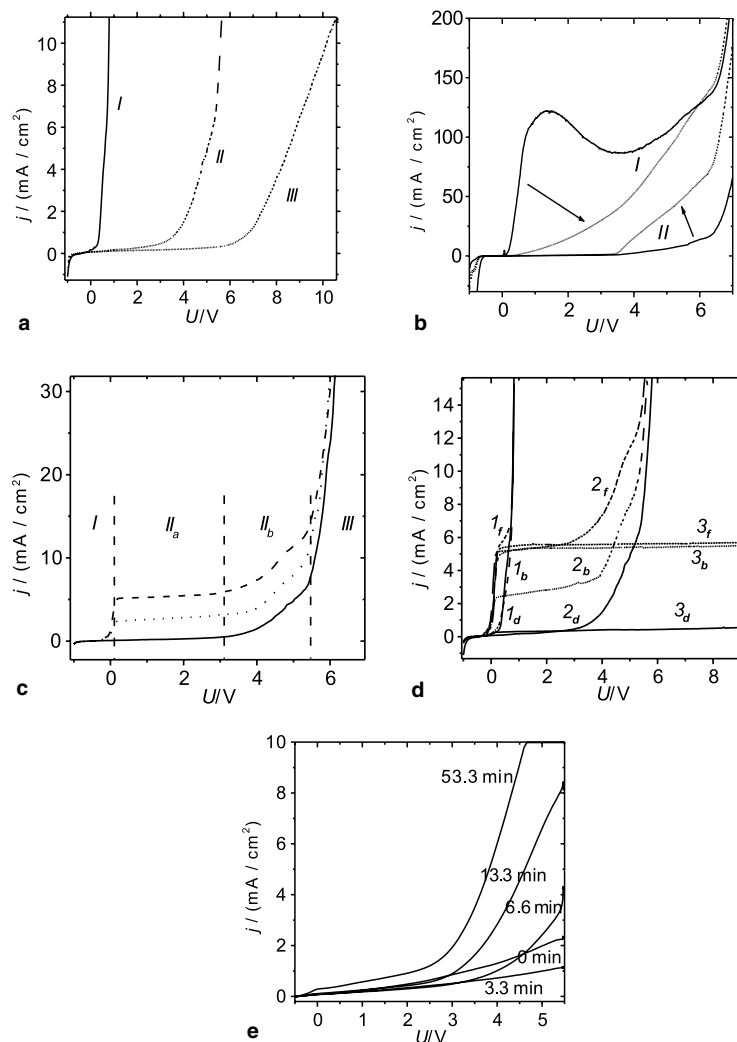


Fig. 2. *IV* curves of the Ge–HCl contact. Ge sample: 0.15 Ω cm (medium doped), thickness 300 μ m. Standard etching conditions, but also with illumination. (a) Differently doped samples in the dark. High (I), medium (II) and low (III) doped sample, respectively. (b) Medium doped samples in the dark, dependence on the surface roughness. I: abraded (i.e. mechanically damaged) surface; II: rough surface (back side, no mechanical damage). Arrows indicate the shift of the *IV* curves with the repeated potential scanning, i.e. with etching time. (c) Medium doped in the dark (solid line), and with front side (dashed line) and back side (dotted line) illumination. (d) Photo current dependence for different doping levels. High (1), medium (2) and low (3) doped samples, respectively. Footnotes (b,d,f) denote darkness, back side or front side illumination, respectively. Sample 2 has a good, sample 3 an excellent diffusion length, whereas sample 1 does not show a bsi effect. (e) Quick *IV* curves. Scan rate = 20 V/s, Ag/AgCl reference electrode, medium doped sample (0.17 Ω cm). (0 min means the first *IV* measurement).

For these standard conditions, the following features were observed:

- (i) Junction breakdown, i.e. a rapidly (e.g. exponentially) increasing current vs. applied potential is always achieved at a few volts (usually 3–5 V), independent of the doping, cf. Fig. 2a). This is more reminiscent of the III–V's, in particular GaAs, where breakdown occurs at relatively low voltages, too, than of Si, where breakdown conditions for low-doped samples typically require external voltages of 100 V and more.
- (ii) In semiconductor junction terms, there is often an appreciable leakage current that increases with the voltage before breakdown occurs. This may also take

the form of three distinct regions (see Fig. 2c), consisting of a region I with very low current even under illumination, a region II with constant leakage current (and on occasion a portion IIa showing a linear increase of the current), and finally a region III where breakdown occurs. The details of region IIa depend on etching time and thus on the developing pore structure. The effect of illumination is only pronounced in region II.

- (iii) The effect of illumination is reminiscent of Si. All samples show a strong photo current under front side illumination (fsi) conditions, and a more or less pronounced photocurrent under back side illumination (bsi) conditions. The photocurrent induced in the bsi mode can be rather large (e.g. about 1/2 or more

of the photo current induced in the fsi mode, cf. Fig. 2d), indicating very large diffusion lengths in the order of mm, and well passivated back sides. Contrariwise, it can also be small or hardly existent indicating small diffusion lengths, “bad” back sides, or both.

- (iv) The IV curve changes markedly during pore etching. While this is evident from many indirect observations, a systematic study is difficult because the slow voltage scans needed to produce near-equilibrium characteristics change the pore growth mode. A “quick IV ” technique was therefore developed and implemented in additional hard- and software that allows recording a (non-equilibrium) IV curve in far less than 1 s. Such quick IV measurements are not visible in the pore morphology; an example is shown in Fig. 2e.

Pore etching at constant current or voltage always requires a working point in region III or region IIa, respectively, of the IV characteristics, at least for parts of the etching process. In pronounced contrast to Si, no pores are generated if etching is started using only the photocurrent induced by bsi conditions.

Pore etching in Si (and in III–V semiconductors) generally proceeds very differently for low- and high-doped samples. Much simplified, in high-doped Si of both types (n^+ and p^+ samples) always (heavily branched) mesopores are obtained while low-doped samples of both doping types yield micro-, meso-, and macropores in a plethora of morphologies. In III–V semiconductors, the influence of the doping level on the pore morphology appears to be less pronounced, but pore geometries still are more or less directly tied to the width of the space charge region and thus to doping.

It is thus of interest to ascertain to what extent the donor concentration influences pore etching in n-Ge. The result, again unexpected, is simple: so far no clear-cut influence has been found. This statement does not ascertain that there is no influence of the doping level on pore parameters, just that no pronounced influence has been found in the particular region of the parameter space probed so far.

3.2.2. Nucleation and some effects of nucleation on the final pore structure

In general, the geometry (average distance and diameter) and morphology (straight, branched, prismatic, etc.) of pores in semiconductors obtained after typically hours of etching depend very much on the initial nucleation processes. While this is true for all semiconductors, the general experience with Si and the III–V's semiconductor is that nucleation of pores is either easy and pores grow uniformly wherever they happened to nucleate (in particular true for macropores in Si), or that a steady-state with respect to a certain pore geometry is reached relatively quickly, even for different nucleation conditions. The first observation translates in the ability to govern nucleation within a wide

process window by lithographically defined nucleation sites (“seeded” nucleation, now a standard technique for obtaining defined macropore structures in Si); the second observation (unfortunately) renders lithographically defined nucleation almost useless, because the final pore structure is rather independent of nucleation conditions.

As a general finding, pore structures in Ge are far more sensitive to nucleation conditions than pore structures obtained under comparable conditions in Si or InP, at best they are somewhat reminiscent of GaAs. We will first treat the “standard” case of pore growth on a polished surface. The doping level will be specified in the figure captions, but it appears to have no, or only a small influence on the results obtained so far.

During the anodization of low-doped polished Ge samples at current densities $j > 2 \text{ mA/cm}^2$ in the dark (implying that the necessary hole supply comes from some generation process at the pore tip), pores usually grow at a very low density in a more or less inhomogeneous way [19] (again, in marked contrast to Si). Frequently pore domains are formed, because around an initially nucleated pore (central pore), new pores (surrounding pores) will nucleate somewhat later, and then the process continues; thus the whole system forms a distinctive pore domain. An example of a single well-expressed pore domain obtained at $j = 2.5 \text{ mA/cm}^2$ is shown in Figs. 3a and b in top and cross-sectional view, respectively. Normally, the central pores are the deepest ones; whereas the depth of the surrounding pores decreases with distance from the central pore (see Fig. 3b). Fig. 3c shows many overlapping domains at a lower magnification. All pores have $\{110\}$ type walls (and thus a square cross-section), at least near the sample surface, and grow in the $\langle 100 \rangle$ direction perpendicular to the surface.

Pore domains of some kind have been reported earlier in GaP [47], InP, and GaAs [11,40,48]. However, the morphology of the domains in Ge is totally different from what was observed in other semiconductors. This is caused by several factors, in particular by the different crystallography and nucleation behavior of pore growth in Ge compared to that of GaAs or GaP, as will be discussed later on.

The first major experimental task is thus to find conditions for more homogeneous nucleation. With some experience from other semiconductors, one would tend to use large current densities and/or voltages at the beginning of the experiment. This, however, is counterproductive for polished Ge. Somewhat unexpectedly, it proved to be possible to increase the nucleation density of pores in polished samples, and thus to avoid domain formation, by anodizing the samples at very low current densities. This somewhat counterintuitive measure worked best at $j = 0.5 \text{ mA/cm}^2$, the effects of the current density on pore nucleation homogeneity are shown in Fig. 3d.

The size distribution of the pores shown in Fig. 3d is given in Fig. 3f), it is typical for many pore structures. The size distribution of the pores shows two pronounced maxima (on occasion 3 maxima can be found) clearly

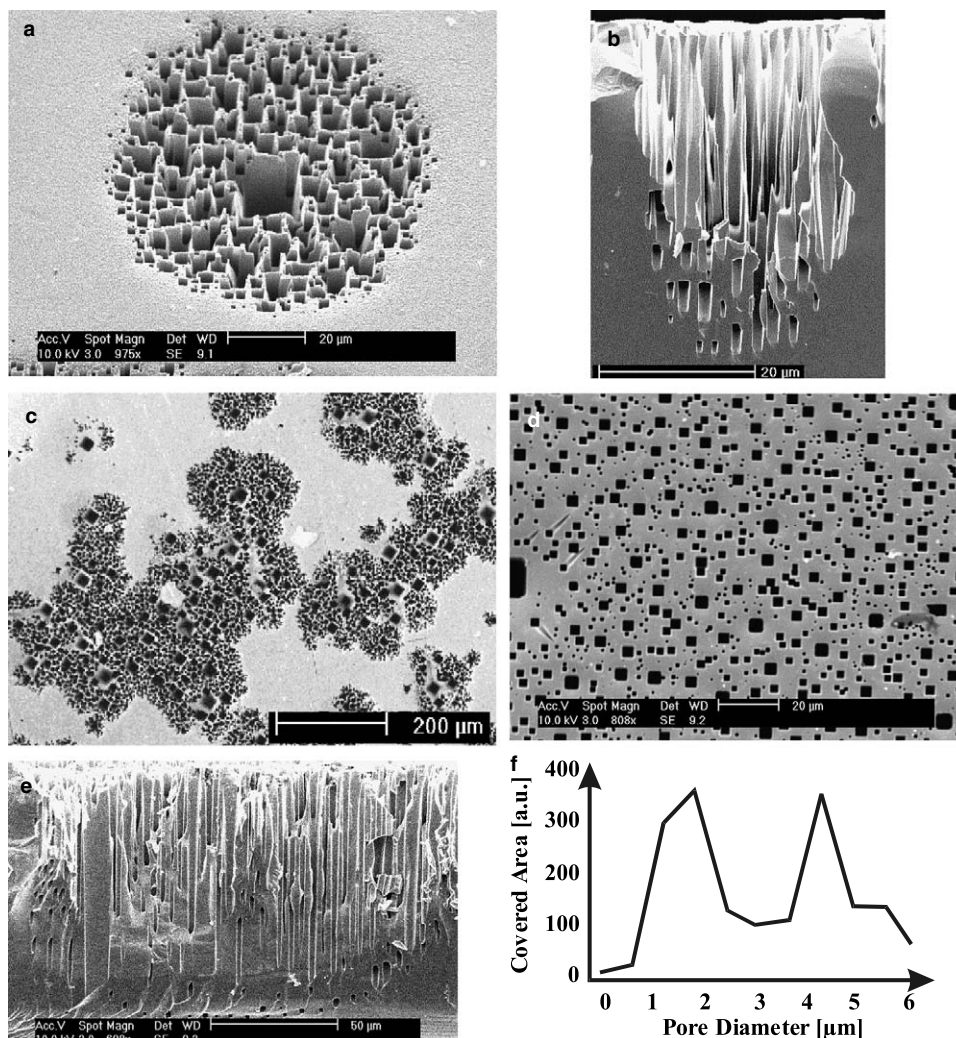


Fig. 3. Pore domains on polished surfaces and dependence on the etching current. Standard etching conditions for lightly doped samples. (a) Single domain, $j = 2.5 \text{ mA/cm}^2$. (b) Cross-section to (a), showing a decreasing pore depth with distance to the center. (c) Overview with clustered domains, $j = 2.5 \text{ mA/cm}^2$. (d) Larger and more homogeneous pore density at lower current density $j = 0.5 \text{ mA/cm}^2$. (e) Cross-section to (d); note the inhomogeneous depth distribution. (f) Pore size distribution to (d).

implying that pores nucleate in “waves” and that their sizes are simply a function of their “age”. This is mirrored in the depth distribution, which is quite inhomogeneous, too (Fig. 3e).

The situation changes markedly if unpolished samples (back side of polished samples with a rough but undamaged surface) are subjected to pore etching. In this case the pore density was extremely low for the formerly “high” current density $j = 2.5 \text{ mA/cm}^2$, but no domain formation was observed (Fig. 4a). The density of pores increased, however, with increasing current density, still without domain formation (Fig. 4b). The most uniform distribution of pores for rough surfaces was observed at $j = 7.5 \text{ mA/cm}^2$ (a current density that would only produce some isolated domains on polished surfaces), Fig. 4c). While the pores are now homogeneously distributed, their size still varies considerably, most likely again simply mirroring their individual nucleation times (Fig. 4d).

Thus, best uniform nucleation for polished low-doped Ge samples was achieved at low current densities, whereas for non-polished samples uniform nucleation occurs at high current densities.

The constant electropolishing of the Ge surface tends to render isolated pores into an over-all conical shape since the upper part of a pore has more time to grow in diameter than the lower part. This is visible in the cross-sections above. However, as soon as the thickness of Ge between the pores, i.e. the thickness of pore walls, becomes comparable to twice the thickness of the space charge region present in the Ge for the prevailing conditions, the pore wall is essentially charge carrier-free and then more stable, as will be seen in later pictures. In consequence, pores are no longer conical, or, to be precise, much less so than in the isolated state. All the effects mentioned have not yet been observed in other semiconductors and are rather special to Ge. They may be

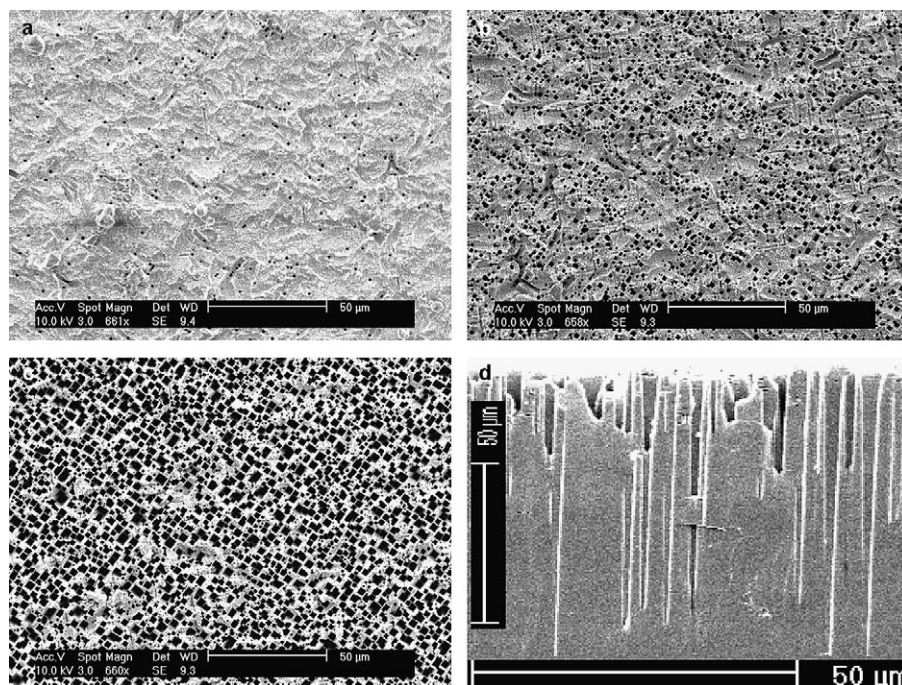


Fig. 4. Pore density on rough surfaces as function of the current density. Standard etching conditions for low-doped sample. (a) $j = 2.5 \text{ mA/cm}^2$, (b) $j = 5 \text{ mA/cm}^2$, (c) $j = 7.5 \text{ mA/cm}^2$, (d) cross sectional view of the pores shown in (c); foreshortened to enhance conical shapes.

understood to some extent from the band structure of Ge, as will be outlined in Section 4.

3.2.3. Growth direction, morphology, and branching

3.2.3.1. Pores growing in $\langle 100 \rangle$ direction. Cross-section of pores growing in the $\langle 100 \rangle$ direction (the “top-view” pictures) invariably shows pores as rather perfect squares, or as squares with truncated corners; the pictures in the figures above illustrate this fact quite nicely. The major stable facets of a pore are clearly $\{110\}$ type planes, a unique feature of Ge never observed in other semiconductors until very recently in GaP [49]. In addition, $\{100\}$ planes may form the truncated corners of $\{110\}$ sided cylinders, as illustrated in Fig. 5a. That the pores discussed here are crystallographic in nature (“crysto” pores) and not current-line pores (“curro” pores, see chapter 3.1), something not directly distinguishable for $\langle 100 \rangle$ pores in a $\{100\}$ substrate, is shown in Fig. 5f), where $\langle 100 \rangle$ oriented pores are shown in a $\{115\}$ oriented substrate.

Pits in the shape of inverted pyramids usually precede pores, while electropolishing of the surface often leaves real pyramids behind. On $\{100\}$ samples two kinds of crystallographic pyramids can exist and are experimentally observed: Pyramids with $\{111\}$ sides (“ $\{111\}$ pyramids”) or with $\{110\}$ sides (“ $\{110\}$ pyramids”). If a pore is formed by one of these (inverted) pyramids wandering into the depth of the sample along the $\langle 100 \rangle$ direction perpendicular to the surface, the pore walls are either of $\{110\}$ or $\{100\}$ type for the $\{111\}$ or $\{110\}$ pyramids, respectively. The initial shape will change, however, due to lateral

pore growth by electropolishing, and this may produce a switchover from one kind of pore wall to another one. Since a growing pore needs a relatively sharp tip, and since it is not possible to construct a (prismatic) pore with a tip made completely from $\{110\}$ planes, the system compromises: A $\{110\}$ -pyramid grows into the depth, and lateral growth changes the resulting $\{100\}$ planes to $\{110\}$ planes wherever possible. However, since substantial lateral growth is only possible if a pore has no immediate neighbors, individual pores may behave differently. In summary, complicated morphologies as shown in Figs. 5c–e may result that depend on many parameters.

The constant electropolishing on top of the anisotropic pore growth causes the surface of a porous layer to move into the depth, just at a lower speed than the pore tips. If the major pores have side pores, the regressing surface will expose these side pores whenever it cuts through them (schematically indicated in Fig. 6d). That this is indeed the case on very different length scales is shown in Figs. 6a–c, where side pores growing in $\langle 100 \rangle$ directions parallel to the surface (and with $\{110\}$ walls) are exposed.

The side pores also grow in $\langle 100 \rangle$ directions and have the by now expected conical shape. These side pores are not contained in “clean” $\{110\}$ cleavage-plane cross-sections and therefore hard to observe, except for rare occasions as shown in Fig. 6d. This figure is an important reminder of the fact that top-view pictures plus cross-sections with a $\{110\}$ -cleavage plane do only show part of the structures, and that the usually “invisible” side pores might be an integral feature of pores in Ge.

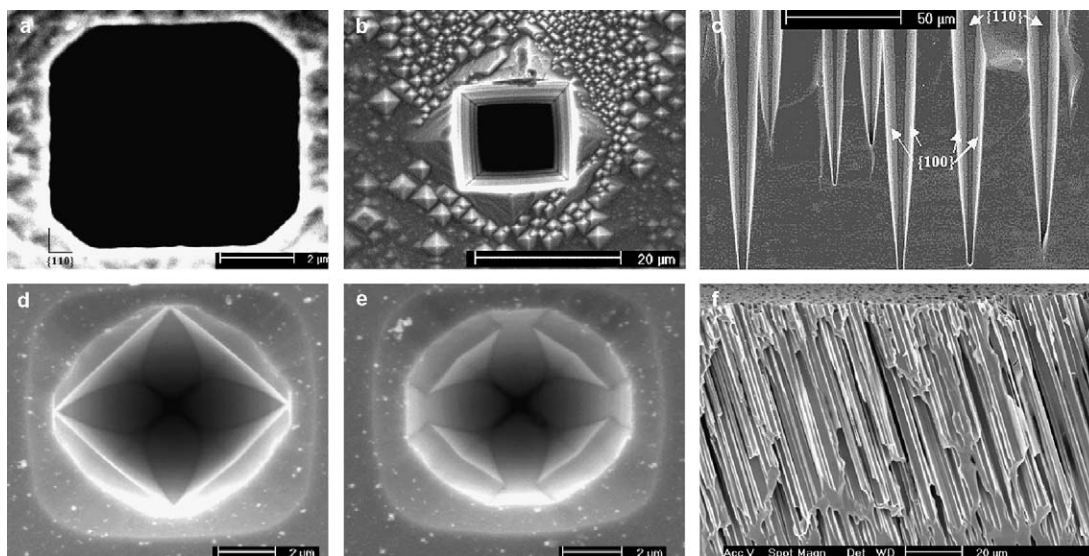


Fig. 5. Crystallography of pores obtained on a $\{100\}$ surface under different etching conditions. For details see text. (a) Top view of pores with octagonal shape formed by $\{110\}$ and $\{100\}$ side walls. (b) $\{110\}$ pore on top of a $\{110\}$ pyramid. (c) Cross-section of pores with octagonal shape. The darker pore walls are $\{110\}$ oriented, while the brighter ones are of $\{100\}$ type. (d), (e) Complicated morphologies of (nascent) pore tips showing change-over from $\{111\}$ pyramid tip to $\{110\}$ pyramid. (f) Pores in a $\{111\}$ oriented substrate proving that the pores are of “crysto” type.

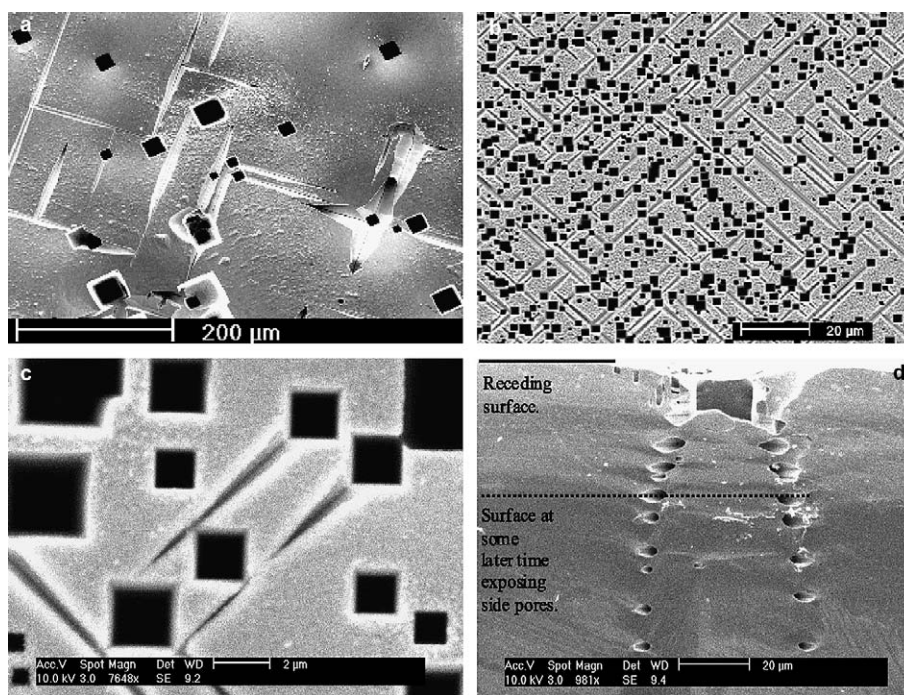


Fig. 6. Side pore development under standard etching conditions (low and medium doped). (a–c) Side pores rendered visible by continuous electropolishing of the surface. (d) Cross-section showing side pores emerging from a large pore, which is visible at the top but obscured farther down due to uneven cleavage.

As in all other semiconductors, side pores are only able to grow if there is sufficient space between the pores; this is evident when comparing Figs. 6a and b.

3.2.3.2. Pores growing in $\langle 111 \rangle$ direction. At present, there are far fewer observations of pores growing in the $\langle 111 \rangle$

direction as compared to $\langle 100 \rangle$ pores. As a rule of thumb, $\langle 111 \rangle$ pores are observed either for organic electrolytes in both n- and p-doped substrates (see chapter 3.5), or for n-doped samples in aqueous electrolytes and large HCl concentrations. To what extent other parameters like doping or the temperature influences the preferred growth

directions remain somewhat unclear at present. High doping levels, however, seem to encourage $\langle 111 \rangle$ growth directions, in particular during the end of the etching process.

Raising the Cl^- concentration from 1.5 to 5 mol/l by adding KCl to a 5% HCl aqueous electrolyte also induces $\langle 111 \rangle$ growth directions, cf. Fig. 7d.

Fig. 7 shows some examples of $\langle 111 \rangle$ pores. The cross-sections of $\langle 111 \rangle$ pores are not always well defined and may appear triangular, oval or roundish, cf. Figs. 7a and c. In the examples given it can be surmised that pores grow in all four $\langle 111 \rangle$ directions (including downwards and upwards growth), but this is not always the case. In fact, as will be shown later, on occasion a new kind of domain structure can be observed where each domain contains pores growing predominantly in only one of the available four directions.

More about $\langle 111 \rangle$ pores will be found in the following chapters dealing with $\{111\}$ oriented samples and organic electrolytes.

3.2.4. Illumination effects

The holes necessary for anodic etching of n-type semiconductors are either recruited from the minority carriers present in thermal equilibrium in the n-type samples (producing what will be called “leakage current”) or must be produced in non-equilibrium either by some kind of breakdown of the space charge region (e.g. avalanche or tunneling) or by illumination. Illuminating the front side (front side illumination or fsi mode) can generate arbitrarily large

hole concentrations close to the reactive surface, directly given by the number of photons being absorbed. However, these holes have to diffuse progressively deeper into the sample to reach the pore tips, and as a consequence fewer holes will reach the pore tip with increasing pore depth. For typical pore depths larger than the diffusion length of the holes (e.g. in all III–V’s), the fsi mode therefore is considered not to be conducive for pore growth. While the situation is not quite that simple in Si (cf., e.g. [14]), fsi illumination had little effect on pore growth in III–V semiconductors, indeed. A few fsi-mode experiments with Ge failed to produce any pores, and we will not pursue the fsi mode for Ge anymore, except as a kind of calibration for the far more interesting back side illumination or bsi mode.

Back side illumination under conditions where the holes produced at the back side can reach the front side is thought to stabilize growing (macro) pores for the following reason: Small pits originating from (residual) surface roughness or from the first stage of dissolution will always bend the equipotential surfaces in the space charge region in such a way that holes, which are diffusing in from the back side of the sample, will be focused to the tips of pores or pore nuclei. In consequence, for optimized pore geometries, only the pore tip will draw current, and pores, after successful nucleation, should grow perfectly stable through the whole sample. This is the base of the so-called n-macro (bsi, aqu) pores in Si with their many remarkable properties and potential uses (cf. e.g. [50,51] for some recent work not yet contained in [14]).

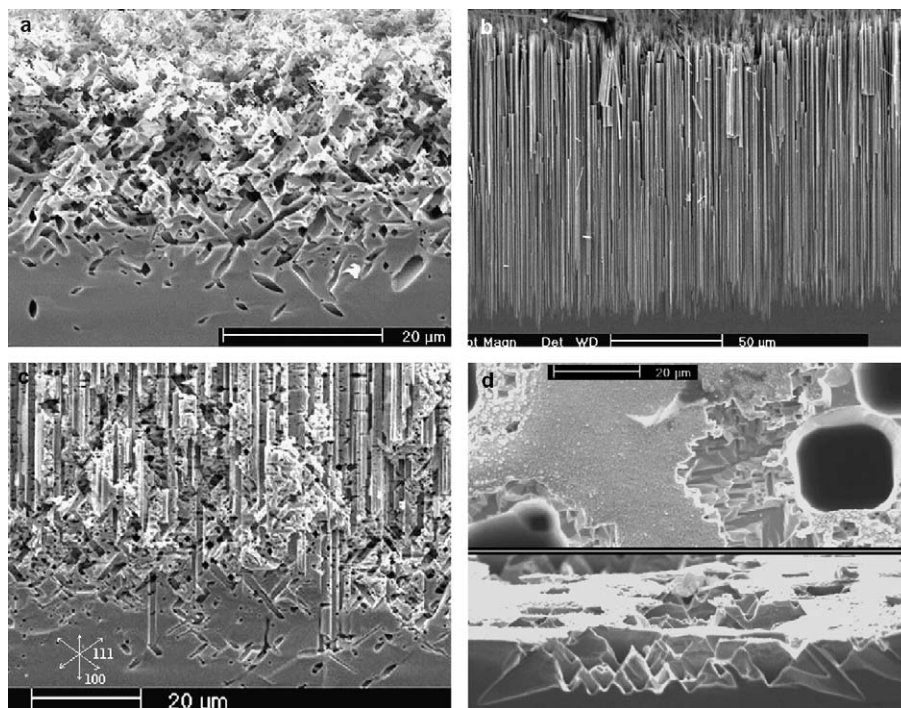


Fig. 7. Pores growing in $\langle 111 \rangle$ directions in $\{100\}$ samples. Standard etching conditions for high (a–c) or low-doped (d) samples, but deviating concentrations of HCl in an aqueous electrolyte and temperatures as indicated. (a) 10.7%, $T = 14^\circ\text{C}$, 1050 min (ramped current); (b) 2.7%, $T = 14^\circ\text{C}$, 1050 min (ramped current) for comparison; only good quality $\langle 100 \rangle$ pores are observed. (c) 5%, 900 min, ramped current; branching from $\langle 100 \rangle$ to $\langle 111 \rangle$ occurs. (d) Top view and cross-section of pores obtained in 10.5% HCl (aqu) + 20% KCl for medium doped sample. $T = 24^\circ\text{C}$, 120 min (ramped current).

Back side illumination produces a defined number of holes, which would give rise to a maximum current density j_{illu} if all holes would be collected as current. Some of the holes generated will diffuse to the tip of a growing pore, which is a distance $d - d_{\text{pore}}$ away from the sample back side, and d is the thickness of the sample and d_{pore} is the pore depth. Neglecting recombination at the back side surface or interface, the holes recombine after they moved on average a diffusion length L away from their “birthplace” at the back side. Therefore only a fraction of the holes generated at the back side will be able to reach the pore tips, where they produce the etching current j_{etch} . The following simple equation obtains for the relation of the number of holes generated and the number of holes producing current

$$\frac{j_{\text{etch}}}{j_{\text{illu}}} = \exp\left(-\frac{d - d_{\text{pore}}}{L}\right).$$

The diffusion length L in indirect-gap semiconductors is a sensitive function of lattice defects, and point defect concentrations in the low ppb range will already be sufficient to render it much smaller than the typical sample thickness in the 0.5 mm region. As a rule of thumb, a (huge) diffusion length equal to the sample thickness produces an etching current of about 1/3 of the illumination current, as follows from solving the diffusion equations for a point source on a (non-recombining) back side [15]. This is the reason why so far only state-of-the-art Si (with diffusion lengths approaching mm) could be etched in the bsi mode; in all other semiconductors investigated so far, diffusion lengths are restricted to the nm– μm region and thus are too small for the purpose.

Since the low-doped samples (which would have been the natural candidates for bsi experiments) were rather thick (about 1 mm), medium doped samples with a thickness of 0.5 mm were used for illumination experiments. However, only some samples showed sufficient bsi photo currents and not many experiments have been performed at present. Examples of the IV -characteristics of illuminated samples with a large diffusion length were already given in Fig. 2d); j_{etch} in this case is about 1/2 or even more of the current density produced by front side illumination for identical illumination conditions. Since the fsi photo

current can be taken as a direct measure of j_{illu} , the samples had excellent diffusion lengths of at least 500 μm . Besides Si, Ge is the only semiconductor with sufficient lattice perfection to allow bsi mode etching at all, and this mode has been tried by the authors for the first time.

From years of experience with Si it is known that bsi-mode etching at a relatively low voltage (i.e. in region II of Fig. 2c) produces well-shaped deep macropores for either potentiostatic or galvanostatic etching conditions. However, Ge is different: For those conditions only electro-polishing was found, no pores were formed, cf. Fig. 8a; this was also true for experiments performed in region I.

Probably the bsi mode in the Ge case is not able to nucleate pores; it was thus advisable to decouple pore nucleation and (hopefully) stable pore growth. A number of experiments were performed in this direction. While pores could be formed again, the result was not convincing.

Best results were obtained if the current is monotonically increased from region I to region III, and then is switched to a constant current in region II for the rest of the time (typically 60 min), as already reported in [52]. Numerous additional experiments with all kinds of parameter variations could not really improve very much upon the early findings and therefore will be omitted.

In total it appears that bsi conditions could be helpful in the goal of producing “good” pores in Ge, but only marginally so. One of the reasons for this is that during etching, the breakdown part of the IV characteristics always moves to lower voltages, obscuring illumination effects (visible e.g. in Fig. 2b). However, despite many attempts, the results of the experiments performed so far do not yet allow us to draw exhaustive conclusions about the effect of a back side illumination, and more work will be needed to clear the issue.

3.3. Special experiments for optimizing pore structures

3.3.1. Improving nucleation

So far, the pores obtained on {100} samples were rather large (diameters of several μm), and their density was low and generally not very uniform. In all other semiconductors run in comparable etching modes (hole supply by

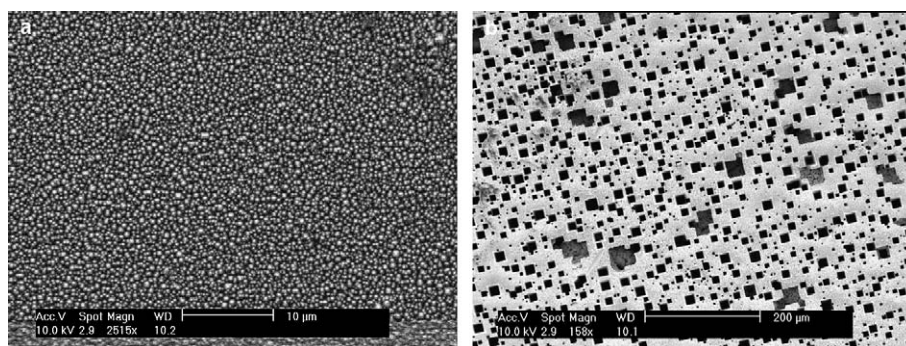


Fig. 8. Pore etching in the bsi mode. Standard etching conditions for medium doped sample but 60 min etching time. (a) $j = 10 \text{ mA/cm}^2$ in the bsi-mode (region II). (b) $j = 40 \text{ mA/cm}^2$ in the bsi-mode (region III).

breakdown or bsi), the pore geometry, in a crude approximation, was mostly linked to the radius of curvature at the pore tip needed to induce breakdown or to the width of the space charge region [15]. The Ge pores do not appear to meet these criteria – they are simply too large. They are also too large for many possible uses, and optimizing pores thus appeared to be a meaningful undertaking. Optimizing, in this context, simply means to produce large and uniform densities of small pores having a uniform depth distribution.

As a first step it is thus necessary to improve the nucleation behavior. While the pore distribution shown in e.g. Fig. 3d looks relatively homogeneous, it is not dense enough and only appears to be uniform because a second or third batch of pores nucleates long after the first batch of pores started growing. The situation may even be worse for other orientations or electrolytes. A number of different methods for improving nucleation was tried; but many attempts did not yield noticeable improvements. Good results were obtained with

- (i) Ramping the current or the voltage in the beginning of the etching.
- (ii) Abrading the surface and thus producing surface damage.
- (iii) Using temperatures above or below room temperature.
- (iv) Combinations of the above.
- (v) Providing seeded nucleation by using lithography.

Many experiments conducted in these directions can be summarized as follows: Abrading the surface with SiC or diamond powder, and/or using a current ramp under galvanostatic conditions produced the best results in medium-doped {100} Ge. With some caution it can be stated that this also applies to other doping conditions and orientations, but there is still plenty of room in parameter space for surprises.

There are innumerable possible experiments: Starting with a polished surface, the rough (but not damaged) back

side, or with surfaces abraded with various grades of slurries. Ramping can be done in the galvanostatic or potentiostatic mode with various ramping times and final currents or voltages, ramping and surface conditions can be combined, and all of this can be done as a function of temperature, too. Space does not permit to discuss this topic in detail; in what follows only some particularly illustrative results will be given.

Fig. 9a shows the “worst” case: Potentiostatic etching at 2 V on a polished surface for 300 min. There are only a few badly developed pores. Abrading the surface with 15 μm diamond or SiC slurry while still keeping a constant potential of 2 V makes a noticeable difference already for 90 min etching time (Fig. 9b), but best results are obtained if abrading and ramping is combined. Fig. 9c shows the pore distribution on an abraded surface for a voltage ramp from 0 to 2 V in 120 min. This result can be generalized to some extent as follows: Rough or abraded surfaces are helpful for a more homogeneous nucleation, but ramping the voltage or the current in some optimized way is essential. Raising the voltage to values larger than 2 V (for the general conditions given) is not helpful and tends to coarsen the pore structure. Current ramping under galvanostatic conditions may be superior to potentiostatic voltage ramping, but this is not a strong statement and open to further insights.

Fig. 10 shows galvanostatic ramping and the influence of the temperature and ramping parameters.

The etching temperature does have a marked influence on pore etching in Si and the III–Vs; cf. [14]. In fact, deep macropores in n-type Si etched in the bsi mode may only be possible if the temperature is lowered (cf. [51]), and temperature changes of a few degrees may already produce noticeable effects. Generally speaking, pores get “better” at lower temperatures. Ge is different once more. Figs. 10c and d demonstrate that the pore size decreases dramatically by raising the temperature by 10 $^{\circ}\text{C}$, a mere 3% in absolute terms. While generalizations should be viewed with some skepticism at this point, it appears that high temperatures in connection with ramping are helpful in promoting uniform nucleation at high pore densities. However, this state-

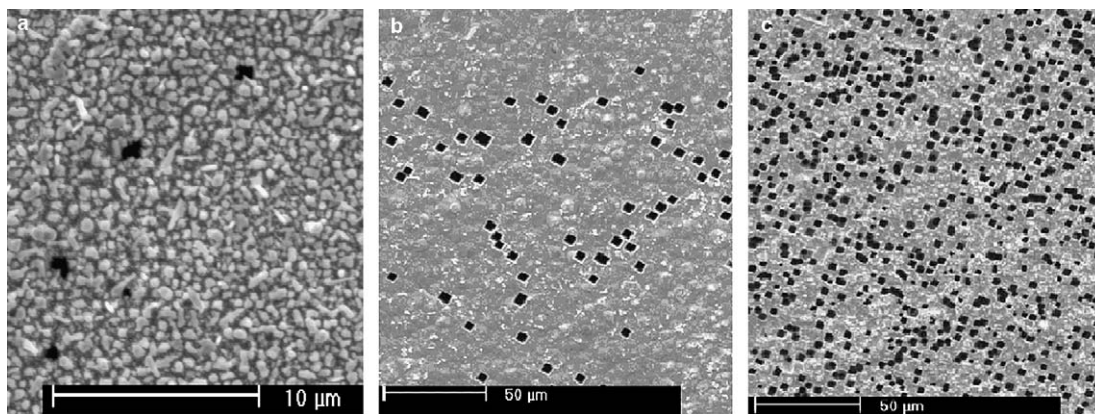


Fig. 9. Nucleation improvement by abrading and ramping. Standard etching conditions for medium doped sample, $T = 18^{\circ}\text{C}$, but: (a) 2 V for 300 min, polished surface. (b) 2 V for 90 min, abraded surface. (c) Ramping 0–2 V for 120 min, abraded surface.

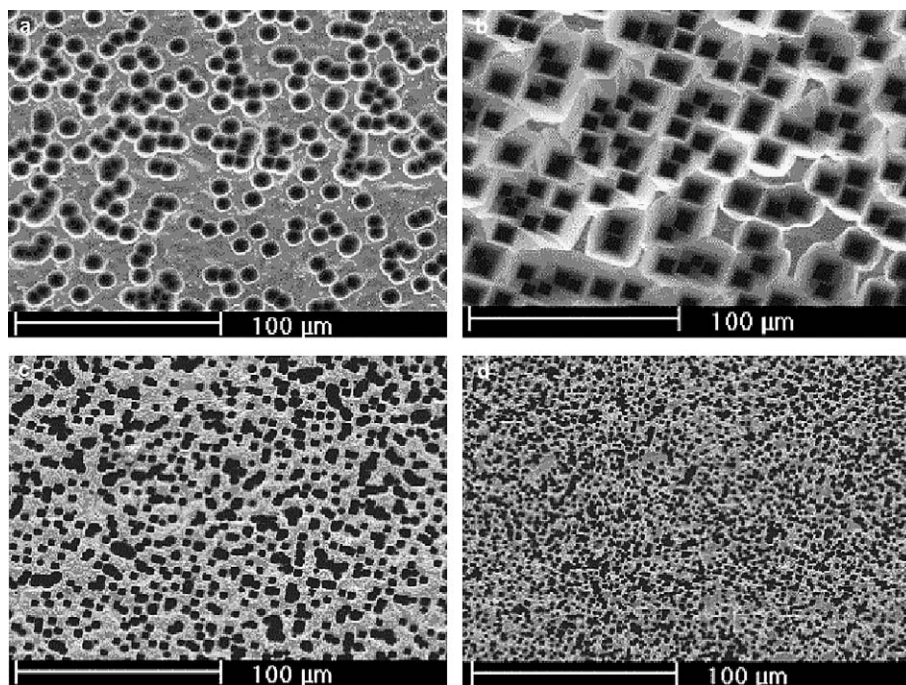


Fig. 10. Influence of current ramping and temperature on nucleation. Standard etching conditions but, (a) 14 °C, linear current ramp 0–15 mA/cm² in a period of 60 min. (b) 14 °C, linear current ramp 0–30 mA/cm² in a period of 120 min. (c) 14 °C, linear current ramp 0–15 mA/cm² in a period of 120 min. (d) 24 °C, linear current ramp 0–30 mA/cm² in a period of 120 min.

ment may not be true for pore growth, where low temperatures may be better for stabilizing pores, i.e. reducing lateral growth by electropolishing. Without current ramping, the effect of the temperature is not as pronounced.

In addition to surface conditioning, ramping and temperature optimization, a short current pulse of e.g. several 100 mA/cm² lasting a few seconds or less may be helpful in improving nucleation. Examples will be shown in later sections.

One attempt has been made to use seeded nucleation by defining a hexagonal lattice of opening in a hexagonal Cr mask with a lattice constant of 2 μm. This experiment was done before some of the results concerning optimization of the general nucleation were known.

The result is shown in Fig. 11b. While generally disappointing, the experiment demonstrated that (i) not all mask openings develop into inverted {111}-type etch pyramids (Figs. 11a and b). (ii) The pyramids that formed are not well localized with respect to the pattern. (iii) Not all pyramids generate pores; cf. Fig. 11a where a large pyramid in the upper right corner did not evolve into a pore, while rather small pores are present around it. (iv) After some etching, inverted {110} pyramids might be found in the proper pattern on the surface together with a few large pores. It remains to be seen if better pattern transfer can be achieved employing optimized nucleation conditions as outlined above.

3.3.2. Stabilizing pore growth

Stabilizing pore growth has two components. First, it requires to keep the pore walls in place, i.e. to avoid lat-

eral growth of the pores in general, and secondly, the conditions at the pore tip (where the only “allowed” growth is to take place) should be kept as constant as possible. Both conditions can never be perfectly met, taken together they limit the possible depth of the pores. Dissolution of the pore walls will eventually lead to pore coalescence; this will first happen at the sample surface where pores had the most time to grow laterally. With increasing pore depth the potential at the pore tip and the concentration of reactants will decrease due to diffusion losses, at the same time the concentration of reaction products will increase. This can never be fully compensated by, e.g., increasing the voltage and the electrolyte concentration, and at some depth the pore will essentially stop to grow.

In Si, where a lot of effort and experience come together, crystallographic macropores (typical diameter <1 μm) with depth >500 μm can be achieved for etching times >8 h or so, and if plenty of “tricks” are used (cf. [51]), while current line pores in InP can be grown through the whole sample (>300 μm) very quickly, very easily, and without any special measures like continuously changing the temperature or the current/voltage).

For n-type semiconductors the (leakage) current flowing through a pore wall is proportional to the concentration of available holes inside the semiconductor times the probability of transfer to the electrolyte, i.e. to some Boltzmann factor describing the effect of the chemical reaction barriers or the degree of pore wall “passivation”. The hole concentration is determined by the semiconductor part of the junction only, while the interface chemistry depends on

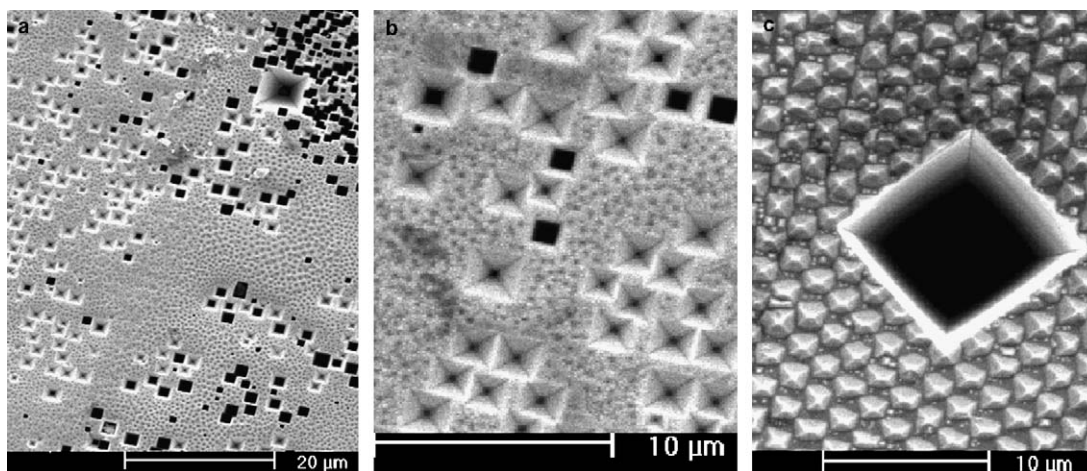


Fig. 11. First result with seeded nucleation under standard etching conditions. The hexagonal lattice of the seed structure is clearly seen in (c). For details see text.

interface conditions and is thus sensitive to the “chemistry”. The available hole concentration for leakage currents is quite different for isolated pores (drawing leakage current from both volume and SCR) and closely packed pores where the pore wall thickness is comparable or smaller than the SCR width. It also decreases exponentially with the band gap and is thus far larger in Ge compared to Si or the III–V’s.

Stabilizing pore growth thus cannot be seen independent of the nucleation. As pointed out before, pores in dense pore arrays do not show conical shapes anymore, because there simply is no space left to grow into, nor do they show side pores for the same reasons. Measures for stabilizing pore growth, besides providing for “good” nucleation, thus consist of essentially two ingredients:

- (i) Increase the current flowing through the tip relative to the leakage currents.
- (ii) Decrease the leakage currents, i.e. provide better passivation for the pore walls.

The first topic includes, e.g., the bsi mode, which allows to produce large tip currents at low voltages, where the leakage currents are still small. However, as described in Section 3.2.4, bsi did not help very much in stabilizing pore growth.

Considering that the leakage currents increase with the pore surface, increasing the total current will at least compensate somewhat for the deteriorating ratio of tip current to leakage current; this measure was tried as shown in Fig. 12.

It can be seen that the lateral growth of the pores was somewhat more pronounced in Fig. 12a compared to Fig. 12b, although the same amount of charge was passed through the samples.

Another possible way to achieve increased surface passivation is to “pulse” the system periodically from cathodic to anodic conditions. Under cathodic bias, the pores would

stop to grow, but the surface might be covered with H^+ , and the additional passivation thus provided might still hold for some time under anodic etching conditions. One might speculate that this was the effect that helped Buriak and Choi [9] to produce pores with their “bipolar” technique.

Fig. 13 shows some results of this technique. An example of the current–time profile impressed on the system is shown in Fig. 13c together with the resulting voltage–time

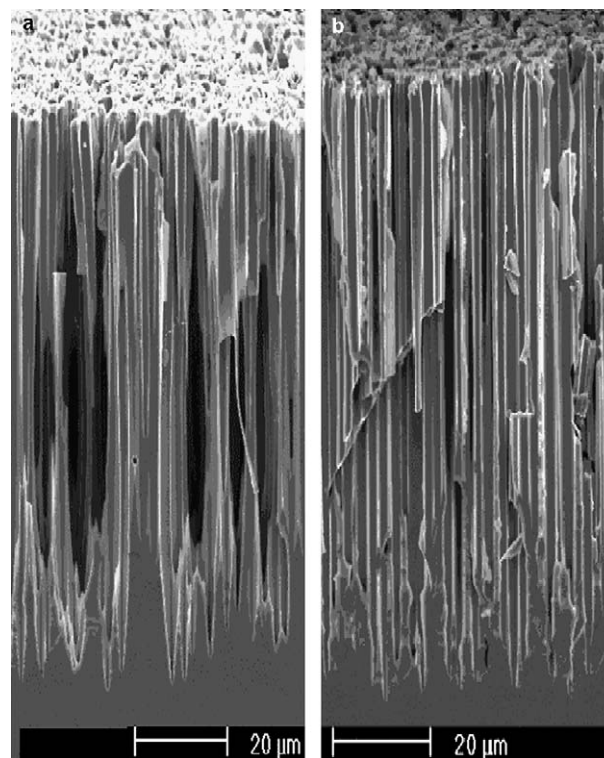


Fig. 12. Pores obtained on abraded surfaces under standard etching conditions, but $T = 24\text{ }^{\circ}\text{C}$. (a) Linear current ramp from 0 to 20 mA/cm^2 in a period of 90 min, then constant 20 mA/cm^2 for 60 min. (b) Linear current ramp from 0 to 30 mA/cm^2 in a period of 140 min.

profile. The pore diameters obtained are quite small, ranging from 0.3 to 3 μm , the (average) diameter is rather constant even for isolated pores. In Figs. 13a and b, the pores show some bamboo-like structure near the tip region, i.e. some “knots” along the pores with an increased diameter resulting from the pulses. It is evident that the pores are not growing in a synchronous fashion; even the number of knots and the average distance between them do not follow a precise pattern. Figs. 13d and e, finally, demonstrate that the cathodic H-passivation, if used from the beginning, also tends to exacerbate nucleation (as expected by now), and that even rather isolated pores do not show the typical cone structure, presumably due to the periodic H-passivation. In contrast, due to some diffusion limitation, pores now tend to increase their diameter near the end of the etching process.

There is a wealth of information concealed in these experiments, but interpretations at present are rather speculative. Nevertheless, the detailed structure of the knots as shown, e.g., in Fig. 13b indicates that some enduring pas-

sivation does occur during the negative current flow. When switching back to positive currents, the pore continues to grow, and it appears that a new tip nucleates at the bottom of the old tip. The “new” tip then grows vertically and laterally, whereas the old tip appears to be rather protected and does not grow laterally as much as the new one.

3.3.3. Making membranes

One of the basic goals of pore etching in Ge was to provide porous Ge membranes for other studies. This, however, proved far more difficult than expected. Nevertheless, based on the body of knowledge reported so far, some attempts at membranes have been made and some results are shown in Fig. 14. In fact, membranes of this kind can now be easily produced in a stirred solution with a three-electrode configuration, in which the sample can be etched from both sides simultaneously.

Fig. 14 shows steps of the membrane production. The etching parameters need to be optimized along the lines shown in the figure caption; it is not sufficient to just etch

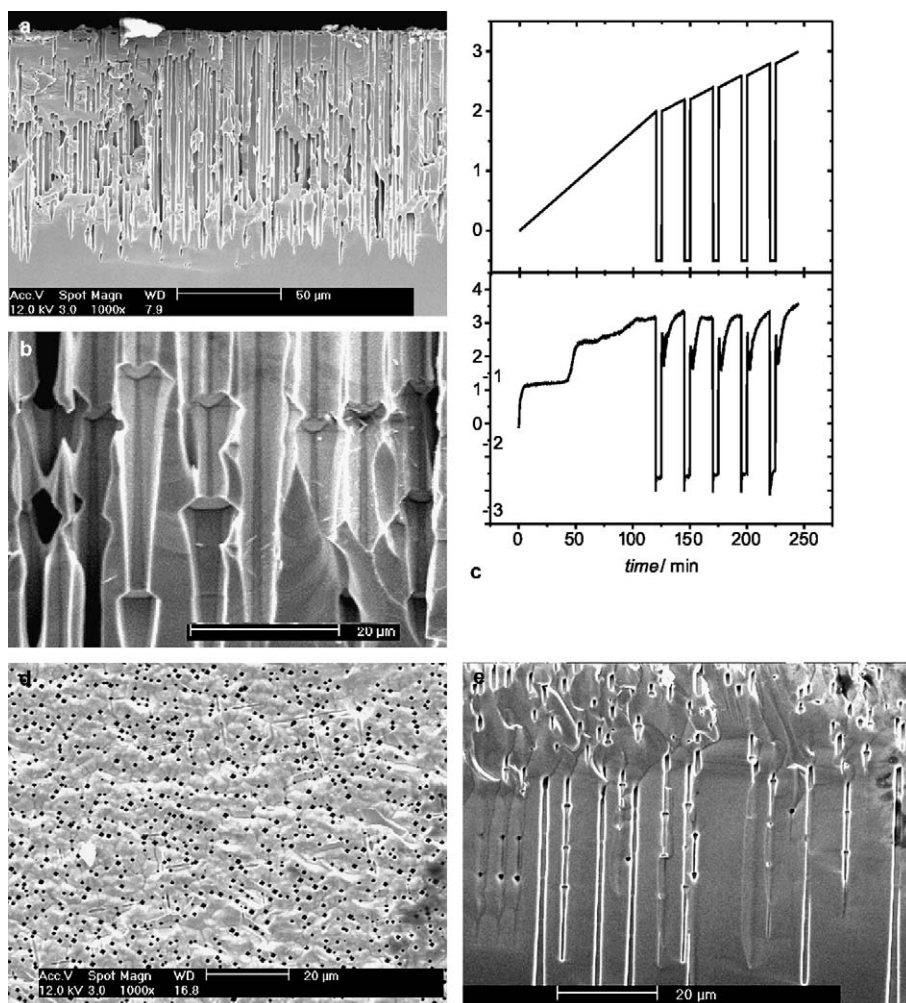


Fig. 13. Pores obtained under standard etching conditions but with pulsing-ramped current. Surface abraded with 1000 mesh SiC powder. (a) High pore density under slow current-ramping slope at beginning. (b) Enlarged view of (a) etched during pulses. (c) Galvanostatically controlled current and corresponding measured potential curves for (a). (d) Relatively low pore density with cathodic pulses from the beginning. (e) Cross-section of (d).

for long times. The surfaces are electropolished all the time; the final membrane thickness thus is smaller than the specimen thickness. Good membranes can also be obtained under potentiostatic conditions, but no details will be given here.

For the sake of completeness, first results of surface state switching from hydrophobic to hydrophilic are shown in Fig. 14d. A finished and contacted membrane was mounted in a glass tube and the flow of water (with the addition of a small amount of H_2SO_4) was measured as a function of the open-circuit potential applied to the membrane. The membrane showed the expected behavior: Under cathodic bias the water flow was strongly reduced, most likely due to H-covered hydrophobic pore walls. Under anodic bias (and presumably OH-covered hydrophilic pore walls), the membrane becomes more transparent to water flow. This effect has been called in the older literature [2], but, to the best of our knowledge, has never been demonstrated before with a membrane. Electrocapilarity and the related effect of electrowetting has found increasing interest in recent years (cf., e.g. a recent review [53],) and the use of a membrane as shown may prove to be of some interest for future applications.

3.3.4. HCl Concentration issues: oxide formation and $\langle 111 \rangle$ pores

Changing the concentration of the “active” part of aqueous electrolytes, i.e. primarily the Cl^- concentration in our standard HCl electrolyte, can be done in several ways, as already pointed out in Section 3.2.3.1. While raising the Cl^- concentration the tendency for the $\langle 111 \rangle$ pore

growth direction increased, lowering the Cl^- concentration (and the temperature) tends to produce pores filled with a substance always appearing bright white in SEM pictures, i.e. a non-conducting substance; some examples are shown in Fig. 15.

The longish substance “growing” out of the pores in Fig. 15a disappears completely upon raising the temperature to 24°C ; the structure then obtained closely resembles the one shown in Fig. 6b. EDX analysis proved what was expected: The pore fillings consist of germaniumoxide, GeO_2 . As can be expected, the water content of the electrolyte is crucial for the oxide formation, too. Substituting water by an organic solvent while still producing pores, has not led to visible oxide formation so far.

While the results graphically demonstrate that macropore formation needs some oxide formation, details are not clear at present. It can be surmised that the formation mechanism of many of the “empty” pores shown throughout this paper is not much different from that of the filled pores, except that the oxide dissolves faster than it is produced; but that is nothing new. However, the unique observation of oxide filled pores in Ge as reported here offers a new window into the study of pore formation mechanisms.

3.4. Organic electrolytes, p-doped samples, $\{111\}$ and $\{110\}$ substrates, and oscillation phenomena

3.4.1. General remarks

While in this chapter a far larger part of the parameter space is probed than in the preceding sections, it is also more “exotic” and will be dealt with in relative brevity.

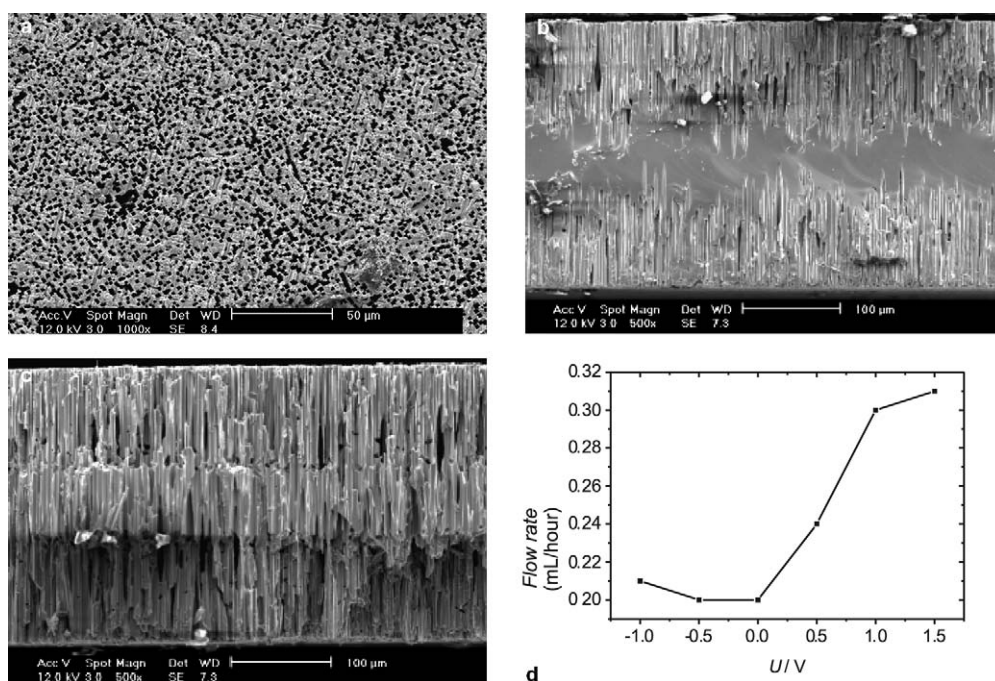


Fig. 14. Porous Ge membrane produced under standard etching conditions and linearly ramped current, but etched from both abraded surfaces simultaneously. (a) $0\text{--}12.5\text{ mA/cm}^2$ in 240 min, then held at 12.5 mA/cm^2 for 40 min. (b) Cross-section of (a). (c) Cross-section after further etching a specimen obtained as in a) at 20 mA/cm^2 for 60 min. (d) Result of an electro-wetting experiment in 1% H_2SO_4 aqueous electrolyte, membrane area 0.2 cm^2 . The switching effect is clearly visible.

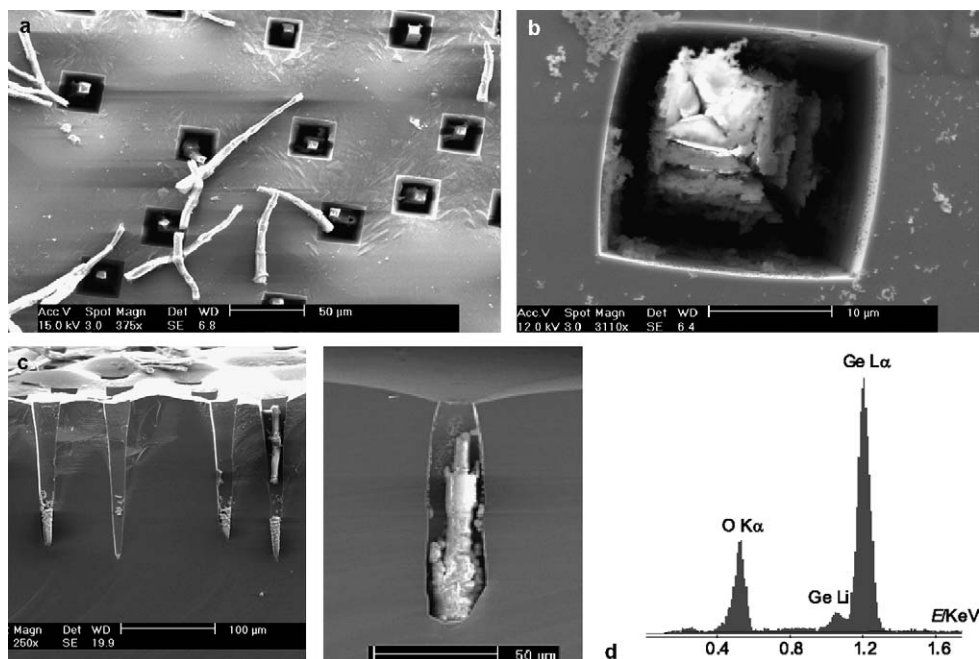


Fig. 15. Standard conditions, heavily doped, (0–3 mA) ramping for a period of 60 min. Aqueous electrolyte with the following compositions and concentrations: (a) 14 °C, 2.7% HCl. (b) 14 °C, 7% KCl. (c) Cross-sectional view of (a) (left) and magnified view (right). (d) EDX spectrum of the substance filling the pore in (b).

From porous Si research it is known that “organic” electrolytes, e.g., electrolytes where the active species (HF in the Si case) is not diluted with water but with some organic solvents (e.g. dimethylformamide (DMF), dimethylsulfoxide (DMSO), or acetonitrile (MeCN)) produce new pore types, sometimes with remarkable properties, cf., for example [30,33,43,54]. In particular, “good” macropores in p-type Si can only be produced in organic electrolytes. Most experiments with Ge have been performed with DMSO based electrolytes and in what follows we only refer to this type of organic electrolyte.

P-doped Ge samples [22,23,25] are of interest because it appears that it is generally quite difficult to obtain good macropores in p-doped bulk crystals (see below). Finally, investigations of substrates with “unusual” orientations, i.e. anything not {100}, have also led to unexpected discoveries in the past; most notably, perhaps, the discovery of the {113} pores in Si [55,56].

All possible combinations of the parameters given in the headline, together with variations of the doping, temperature, and nucleation procedures, would by far exceed all reasonable limits of experimental time and publication space; in what follows only a “flavor” of this issue can be given. While it would be premature to claim that all major pore types have been identified and that the results given in what follows are always typical, we do believe that some basic insights are contained in what follows.

3.4.2. N-doped {100} samples in DMSO electrolyte

In a first experiment the percentage of DMSO in the electrolyte was changed from 20% to 87% (i.e. mixing con-

centrated HCl with pure DMSO to keep the electrolyte as water-free as possible). Generally speaking, it appeared that with increasing DMSO concentration pore nucleation becomes more difficult, while the main pore growth direction changes from $\langle 100 \rangle$ to $\langle 111 \rangle$ as soon as the DMSO concentration exceeds 75%. In the intermediate stage a new kind of domain/pore develops that does no longer show strong crystallographic preferences in its morphology. Fig. 16 gives an idea of what is encountered. If a 87% DMSO electrolyte is used, the tendency to inhomogeneous nucleation / domain formation is even more pronounced and the pores grow in $\langle 111 \rangle$ directions exclusively.

Using the methods described before to improve the nucleation behavior produces somewhat more homogeneous results, but the tendency of forming some kind of domain still is clearly visible, Fig. 17a shows an example. Changing from the organic DMSO electrolyte to an aqueous one or vice versa produces the expected result: $\langle 100 \rangle$ pores develop from some of the $\langle 111 \rangle$ pores produced with the organic electrolyte or $\langle 111 \rangle$ pores develop in all four possible directions from the $\langle 100 \rangle$ pores first obtained with an aqueous electrolyte. While the tips of the existing pores do act as nucleation points for a new pore type upon changing the electrolyte, nucleation also proceeds from the surface or from the pore walls.

3.4.3. P-doped {100} and {111} samples in DMSO electrolyte

3.4.3.1. P-doped {100} samples in DMSO electrolyte. So far, well-developed electrochemically etched deep macropores in bulk crystals could not be produced in semiconductors

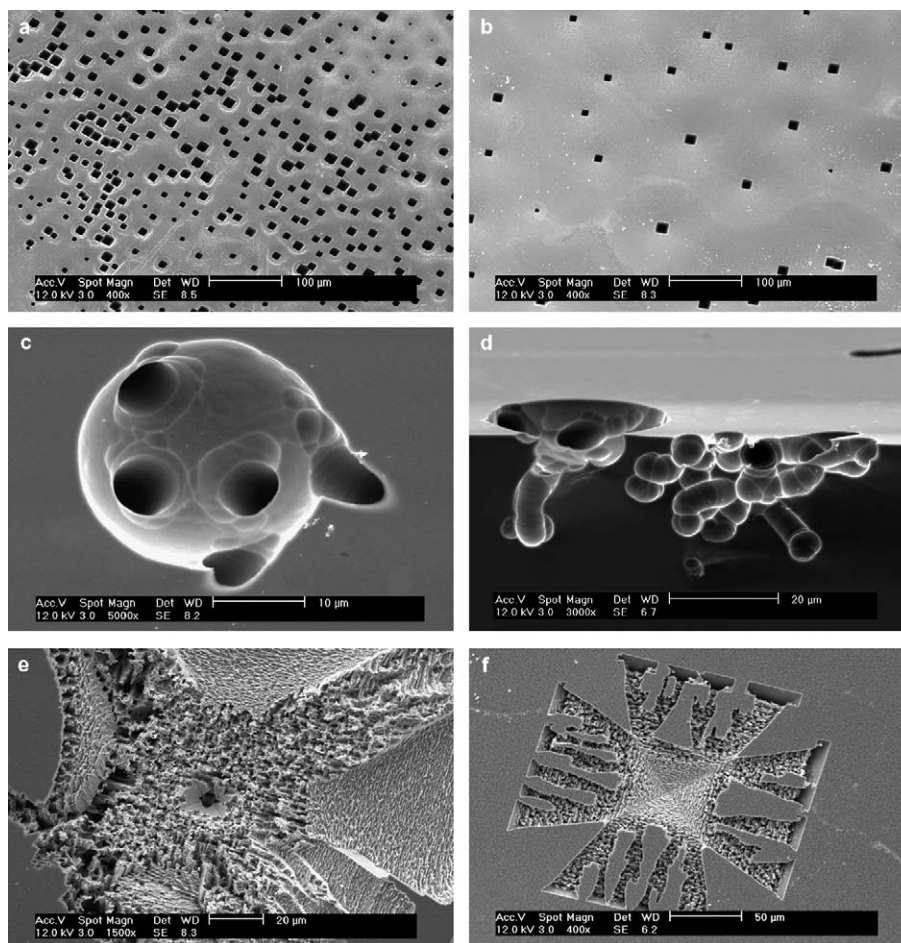


Fig. 16. Changing from an aqueous to a DMSO electrolyte. Standard etching conditions, but linearly ramped current ($0\text{--}5\text{ mA/cm}^2$) in 60 min for (a–c), ($0\text{--}10\text{ mA/cm}^2$) for (d) and (e) for 60 min and ($0\text{--}2.5\text{ mA/cm}^2$) in 30 min for (f). (a) Aqueous electrolyte as reference. (b) 20% DMSO, (c) 75% DMSO, (d) cross-sectional view of (c). (e), (f) 87% DMSO.

other than Si; many attempts (not necessarily published) with, e.g., GaAs, InP, GaP, have failed. An exception to the rule is SiC [57], for some other special cases e.g. in thin films, cf. [13].

In Ge, however, well-developed macropores could be obtained with organic electrolytes as demonstrated in this section. While this is reminiscent of Si where macropores are also most easily produced with organic electrolytes (cf. e.g. [33,43,54]), the pores obtained have many characteristics quite different from those in Si.

Fig. 18 shows a small selection from the results of many different experiments with $\{100\}$ substrates. While the pores obtained share the main characteristics with the n-macro($\{100\}$, org.) pores, e.g. preferred $\langle 111 \rangle$ growth direction or domain formation due to difficult nucleation, they show pronounced differences in detail, e.g. the “carrot shapes” shown in Fig. 18d or very prismatic shapes visible in Fig. 18f.

3.4.3.2. P-doped $\{111\}$ samples in DMSO electrolyte. Considering that $\langle 111 \rangle$ seems to be the preferred pore growth direction in p-type Ge under all conditions, a large number

of experiments was performed with $\{111\}$ oriented substrates. Besides the HCl/DMSO electrolyte many other combinations were tried, too, e.g., HF, HBr, NaOH with DMSO, or HCl with MeCN or DMF. “Good” pores could only be obtained with HCl based electrolytes, and DMSO proved to be superior to the other solvents; therefore only results with HCl/DMSO combinations will be reported here.

As with $\{100\}$ samples, nucleation was extremely inhomogeneous; complicated structures or domains tend to grow laterally from some central primary nucleation point, always accompanied by pores growing into the bulk of the sample. Fig. 19 shows some representative examples.

It appears that large currents correspond to the more roundish pore shapes, while small currents tend to produce prismatic pores. It is also clear that smaller current densities tend to produce pores growing in the available $\langle 111 \rangle$ directions from some central nucleation side, i.e. small current densities tend to induce pronounced domains. This can be clearly seen in Fig. 19d, where a comparatively uniform pore array growing in the $\langle 111 \rangle$ direction perpendicular to the surface transforms into a kind of buried domain

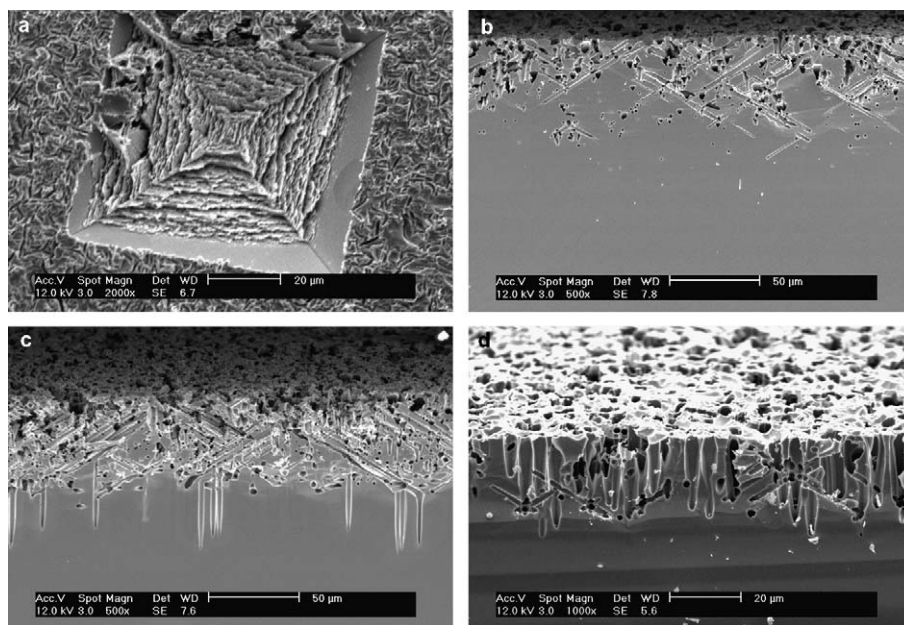


Fig. 17. Top views and cross-sections obtained under standard etching conditions but in 5% HCl/100% DMSO. (a) Abraded surface, top view. 0–2.5 mA/cm² for 60 min increased linearly. (b) Abraded surface, cross-section. 15 mA/cm² for 60 min. (c) Switching from DMSO to an aqueous electrolyte. (d) Switching from an aqueous electrolyte to DMSO.

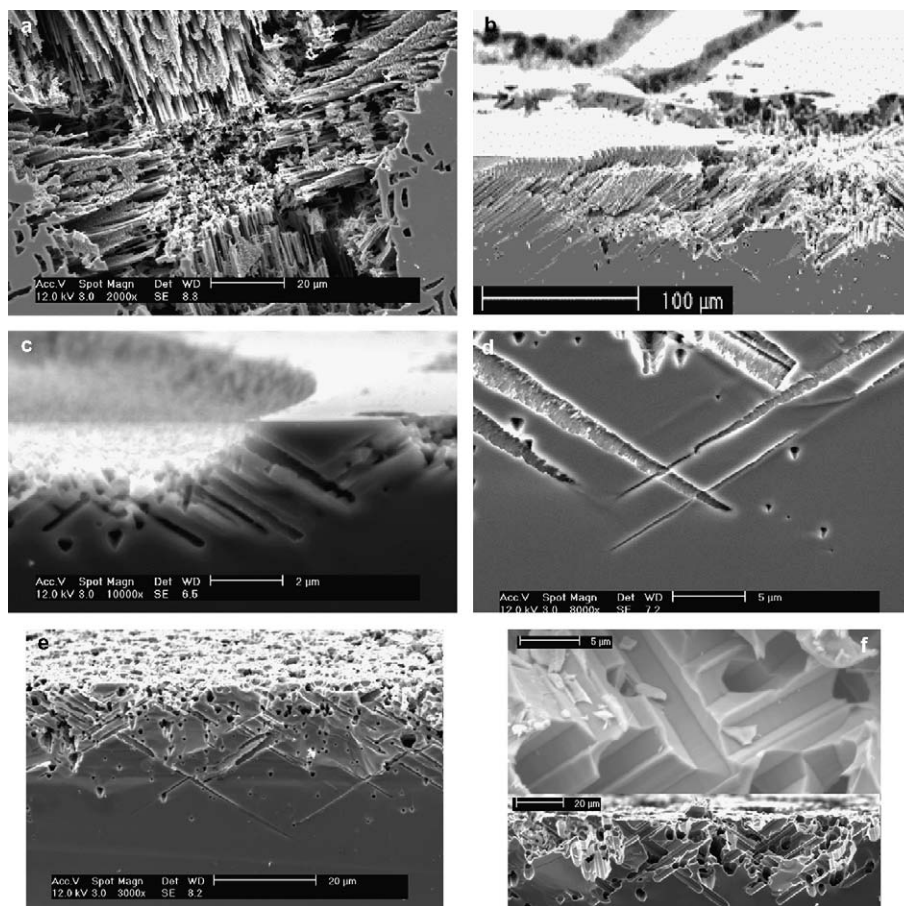


Fig. 18. P-type {100}; doping 10^{14} – 10^{15} cm⁻³, 5% HCl/100% DMSO, 18 °C (dark). (a) Pore domain reminiscent of the one shown in Fig. 17e. (b) Cross-section through a domain. (c) Cross-section through a different kind of domain. (d) Well-developed macropores in (three) $\langle 111 \rangle$ directions. (e) Dense pore structure obtained for 10 mA/cm² for 120 min, rough surface. (f) “Inverse” ramping 10–0.5 mA/cm² in 60 min followed by 0.5 mA/cm² for 600 min, rough surface. Detailed view (top) and overview (bottom).

with pores growing in all four downwards oriented $\langle 111 \rangle$ directions. This kind of sudden changes in the pore morphology with depth (that was also encountered in Fig. 7a) demonstrates that at least one of the chemical reactions involved in pore growth is diffusion-limited in a critical way.

The more pronounced domain formation behavior at low current densities suggested that a more uniform nucleation should be possible by beginning an etching experiment with a “current pulse”, i.e. with a relatively large current for a short time. After that, the current is decreased to the intended current density. This approach worked rather well; it is the reason while in Figs. 19c and d “inverse” current ramps were employed.

There is no strong dependence of the pore morphology and geometry on doping as shown in Fig. 20 as far as that can be concluded on the base of experiments with two doping levels (10^{14} cm^{-3} – 10^{15} or 10^{17} cm^{-3} – 10^{18} cm^{-3} , corresponding to $5.4 \Omega \text{ cm}$ or $0.1 \Omega \text{ cm}$, respectively).

Even prolonged etching (with concomitant electropolishing) does not produce ordered structures (as could have been expected from the Si experience), as shown in Fig. 20c. Despite the nucleation problems, good porous layers and in particular membranes could be produced in p-type Ge, too. In Fig. 20d a membrane is shown to demonstrate the quality that could be achieved.

3.4.4. N-doped $\{111\}$ samples

3.4.4.1. N-doped $\{111\}$ samples in aqueous electrolyte. From the results reported in chapter 3.2 it could be expected that

in $\{111\}$ oriented samples under standard etching conditions three sets of steeply inclined pores would grow in the available $\langle 100 \rangle$ directions. There were two incentives for an experimental verification of this expectation: (i) In the case of Si, the same expectation was proved to be wrong: instead of the expected $\langle 100 \rangle$ -pores, $\langle 113 \rangle$ pores were found [55,56]. (ii) In early experiments [19,58] it was found that it was unexpectedly difficult to obtain pores at all. However, a series of experiments utilizing the better understanding of pore etching in Ge obtained in the meantime, in particular better nucleation procedures, yielded new results as will be described in what follows.

Pores can be nucleated on $\{111\}$, and they grow in all three available $\langle 100 \rangle$ directions under standard conditions plus optimized nucleation; no $\langle 113 \rangle$ pores have been observed so far. On a top-view picture, the threefold symmetry is clearly visible; Fig. 21 shows examples. In samples with a $\{110\}$ cleavage surface, only one set of these pores is contained in the cleavage plane; a typical picture of the set of $\langle 100 \rangle$ pores is shown in Fig. 21c.

Compared to the growth of one $\langle 100 \rangle$ pore at right angles to the surface (i.e. in z -direction) for $\{100\}$ samples, the three sets of pores obtained here grow a factor $\sin 35^\circ = 0.57$ slower into the z -direction. The individual pore growth speed along $\langle 100 \rangle$ is further slowed by a factor of 3 because of the competition of three pores for one “pore current unit”. This leads to a far more severe electropolishing effect as a corollary. In particular, if the surface “grows” faster into the z -direction than the pores, no stable pore growth will be observed.

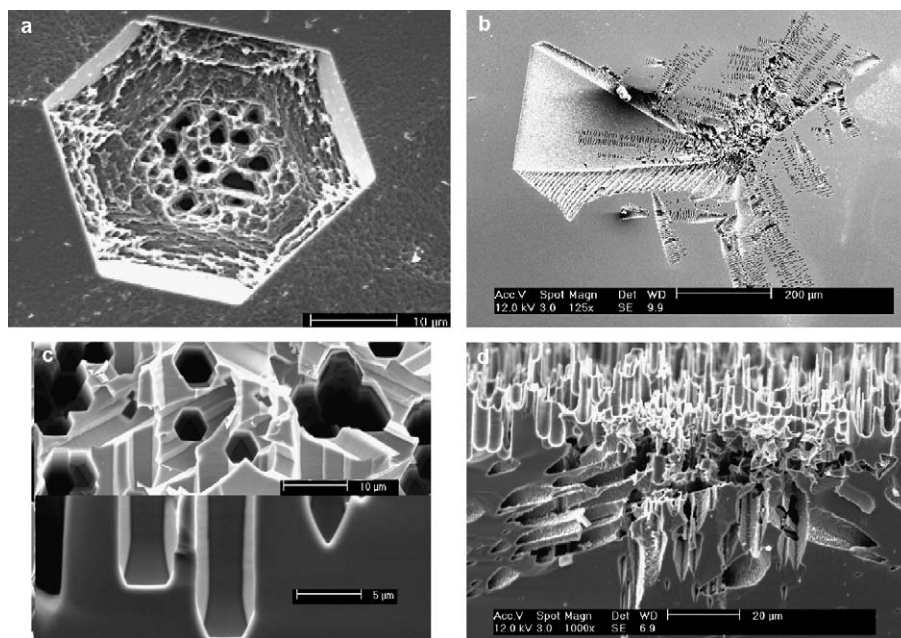


Fig. 19. Pore domains and pores in p-type $\{111\}$ Ge. Doping 10^{14} – 10^{15} cm^{-3} , 18°C , 5% HCl/DMSO electrolyte. (a) Domain formed at low current density. (b) Domain formed at higher current density than in (a). (c), (d) Pores growing in $\langle 111 \rangle$ directions, but with more prismatic (c), or more “roundish” morphologies (lower part of (d)); 0.5 mA/cm^2 for 800 min with ramping from 25 to 0.5 mA/cm^2 in a period of 60 min for (c); 2.5 mA/cm^2 for 300 min, ramping down from 25 to 2.5 mA/cm^2 in a period of 60 min for (d).

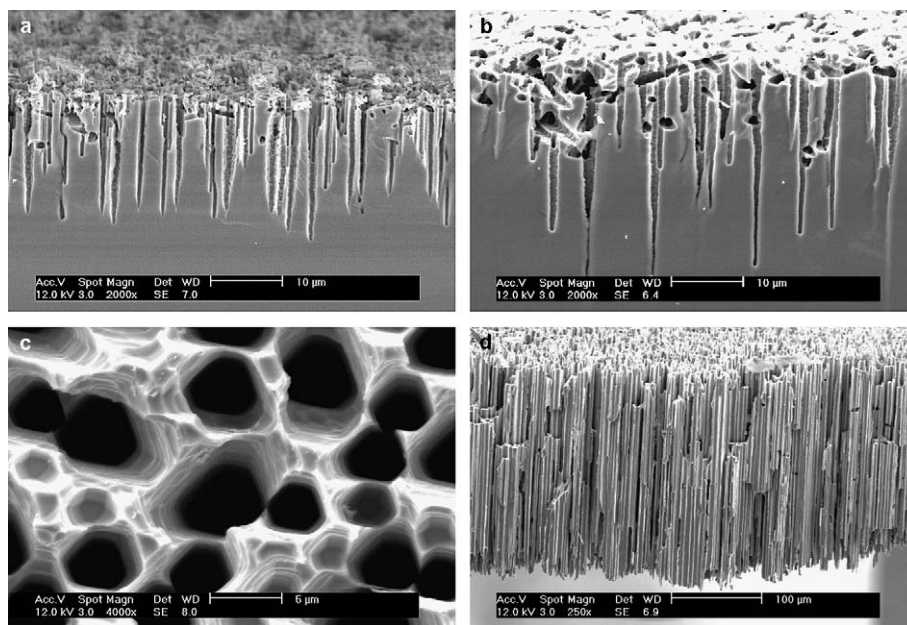


Fig. 20. Pores in p-type Ge. All p-type $\{111\}$, 14°C in 7.8% HCl/DMSO (a) and (b), or 5% (rest). All with current pulse of 25 mA, 6 s at the beginning for improved nucleation. (a) Low doped sample. Ramping down $25\text{--}2.5\text{ mA/cm}^2$ in 60 min. (b) High doped sample. Otherwise like (a). (c) Surface of (b) but after 600 min additional etching at 0.5 mA/cm^2 . (d) Membrane obtained by etching from both sides simultaneously. 400 mA/cm^2 for 12 s, followed by ramping down $50\text{--}5\text{ mA/cm}^2$ in 900 min.

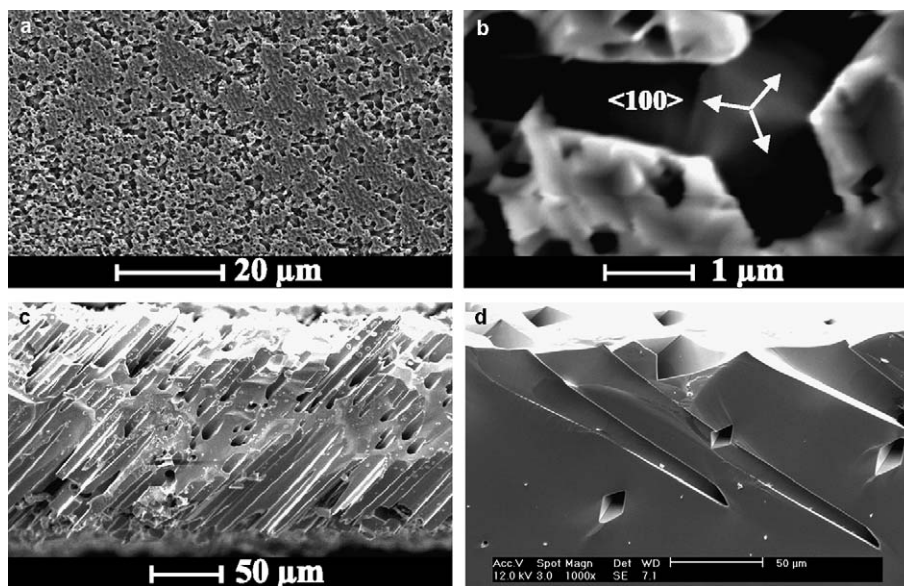


Fig. 21. $\{111\}$ -oriented n-Ge ($n = 10^{15}\text{--}10^{16}\text{ cm}^{-3}$) in the dark under standard etching conditions, but with linear ramping of the current, rough surface, $0\text{--}15\text{ mA/cm}^2$ for 60 min. (a), (b) Top view at different magnifications. (c), (d) Cross-sections at different magnifications. In (d) one set of the inclined pores is visible as diamond-shaped holes ($=\{110\}$ cut through $\langle 100 \rangle$ pores with $\{110\}$ walls).

3.4.4.2. N-doped $\{111\}$ samples in DMSO electrolyte. As in the case of $\{100\}$ samples, it was of interest to investigate the changeover from aqueous to organic electrolytes. The results are shown in Fig. 22. Note that organic electrolytes have a higher resistivity as compared to aqueous electrolytes and thus do not easily allow large current densities at regular voltages. The pores shown in Fig. 22 were obtained at low current densities, and this is the reason

for the difference between the structure shown in Fig. 22 to the comparable one of Fig. 21a. Strong competition between the three crystallographically equivalent $\langle 100 \rangle$ directions for the small current apparently leads to the activation of only one pore growing with a prismatic shape and $\{110\}$ pore walls.

As in the $\{100\}$ case, pores tend to become roundish and “uncrystallographic” for medium to large DMSO

concentrations; for high DMSO concentration they become crystallographic again, with $\langle 111 \rangle$ and $\langle 100 \rangle$ growth directions appearing together. The results obtained for a DMSO concentration in the 70% range are virtually indistinguishable from the once obtained for $\{100\}$ orientation; cf. Figs. 16c and d.

Without special measures (abrading, ramping, temperature,...) the nucleation tends to be rather non-uniform, producing extremely complicated domain structures, some of which are shown in Fig. 23 for medium doped samples. The usually applied current ramping seems to lead mainly to a lateral spreading of the etching process, without generating pronounced pores. The structures produced thus are deepest in the center, where on occasion also some pores may form.

Experiments with constant current devised to counter that effect produced some spectacular structures as shown in Figs. 23c and f.

It is impossible to do justice to the wealth of phenomena encountered in this part of parameter space in just a few pages, suffice it to say that uniformly nucleated good pores

can be produced under optimized conditions; Fig. 24 shows examples.

Smooth “roundish” pores (Fig. 24b) or more prismatic pores (Fig. 24f) can be obtained, essentially as a function of the current density. Large currents (and long etching times) tend to produce roundish pores while smaller currents tend to produce prismatic pores.

3.4.5. N-doped $\{110\}$ samples

Some experiments utilized $\{110\}$ oriented samples, which is of interest for basic research reasons, but also because especially interesting optical properties could be expected for pores in $\{110\}$ semiconductors [59–61]. Only n-type samples with doping in the $(10^{15}\text{--}10^{16})\text{ cm}^{-3}$ range (corresponding to resistivities of 8.5–14.5 $\Omega\text{ cm}$) were investigated in a DMSO electrolyte and in aqueous electrolytes.

In a limited number of experiments it proved to be impossible, however, to obtain pores with aqueous electrolytes in this case, while satisfactory pore growth could be observed for the organic DMSO electrolyte. In what follows only these results will be described.

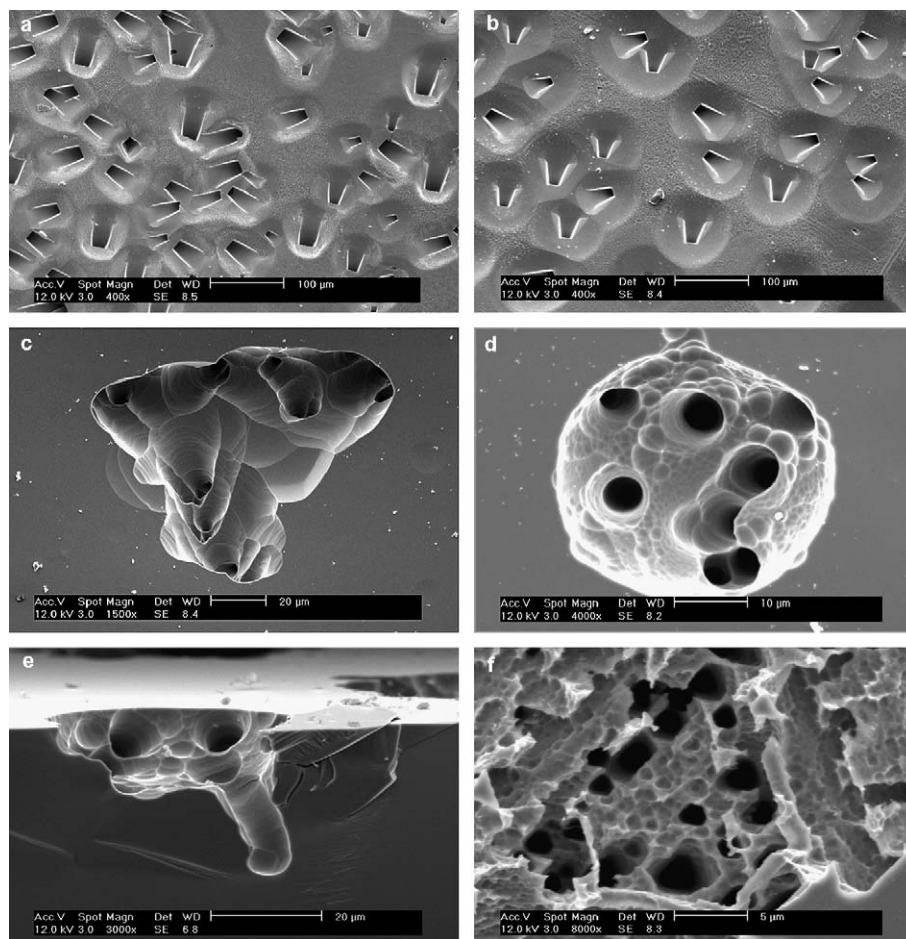


Fig. 22. Changing from an aqueous to a DMSO electrolyte for n-type $\{111\}$ ($n = (10^{15}\text{--}10^{16})\text{ cm}^{-3}$) samples in the dark. $T = 20\text{ }^\circ\text{C}$, polished surface, 5% HCl, ramp current ($0\text{--}5\text{ mA/cm}^2$) (e, f) ($0\text{--}10\text{ mA/cm}^2$) for 60 min. (a) Aqueous electrolyte, (b) 10% DMSO, (c) 50% DMSO, (d), (e) 75% DMSO; (e) is the cross-sectional view to (d), (f) 87% DMSO.

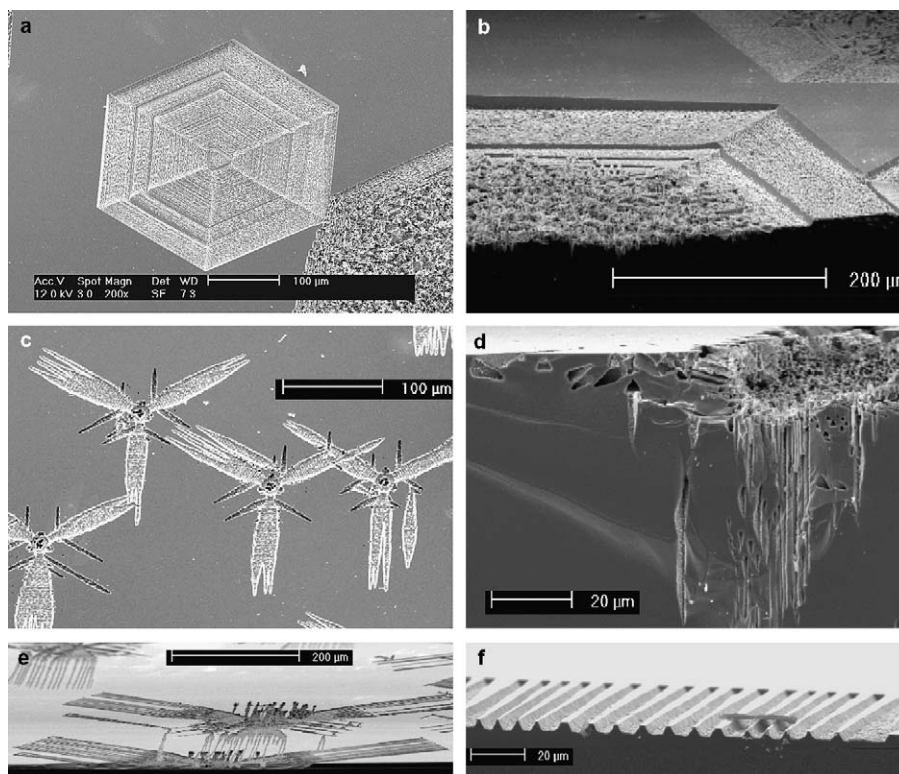


Fig. 23. Domains on n-Ge {111}, $n = 10^{15}$ – 10^{16} cm $^{-3}$, $T = 20$ °C. DMSO electrolyte. All in the dark. (a) Polished surface. Ramping (0–10 mA/cm 2) for 60 min. Hexagonal domain with “growth-rings” and very smooth {110} type edges. (b) Cross-section of (a). Only a few badly developed pores exist in the domain center. (c) Polished surface, kept at 1 mA/cm 2 for 120 min in the dark. “Winged Aliens” domains obtained with constant current etching. (d) Cross-section of (c) taken in the center region. (e) Polished surface, kept at 2.5 mA/cm 2 for 60 min in the dark. (f) Detail to (e), showing pronounced lateral surface structure growth.

The general behavior is similar to the n-macro({111}, org) pores described above – except for the basic crystallography. Both, surface domain geometry and pore geometry, mirror the {110} symmetry, Fig. 25 shows examples. Domains are diamond shaped, again with smooth {110} outer walls or {110} “stop” planes, and pores grow into the depth using the available <111> directions; two of which are contained in the {110} cleavage plane.

3.4.6. Oscillation phenomena

In electrochemical experiments with semiconductors, it is not unusual that current or voltage oscillations are encountered, cf. [62–67]. Most prominent are Si and InP; in the latter case oscillations were sometimes coupled to spectacular self-organization of the pore structure. In the case of Ge, more or less pronounced oscillations were observed in many cases for all kinds of parameters. Fig. 26 shows as one of many examples some self-induced voltage oscillations incurred while doing the etching for the samples shown above in Fig. 25. However, in contrast to comparably well-developed voltage oscillations in the InP case [39,45,68] and very recent observations of oscillations coupled to self-organized pore structures in GaP [49,69], no structure formation or self-organization effects coupled to the voltage oscillations have been observed for the pores so far.

4. Discussion

4.1. General remarks

Researchers who attempted to discuss the pore formation in Si in some detail invariably end up either writing a book [15,16] or at least voluminous papers to some subset of the issue [70–73]. While the total amount of research dedicated to electrochemical pore formation in Ge is miniscule compared to Si, the results obtained so far (and mostly presented on this paper) reveal that the issue seems to be just as complex as in Si; possibly more so because of the added degrees of freedom concerning the choice of electrolytes. It would be tempting, but premature, to present a detailed discussion of all the findings contained in this paper and we will restrict ourselves to a few basic points.

Pore etching in semiconductors combines semiconductor physics and chemistry in a unique way, often with some stochastic physics (or chemistry) and rather involved crystallography and experimental techniques thrown in for good measure. In a purely qualitative and hand-waving way a first statement can be made: While pore etching in n-type Si (and, to a somewhat lesser degree in p-type Si and the III–V’s) relies somewhat more on the semiconductor physics part, pore etching in Ge comes in more heavily on the chemistry side.

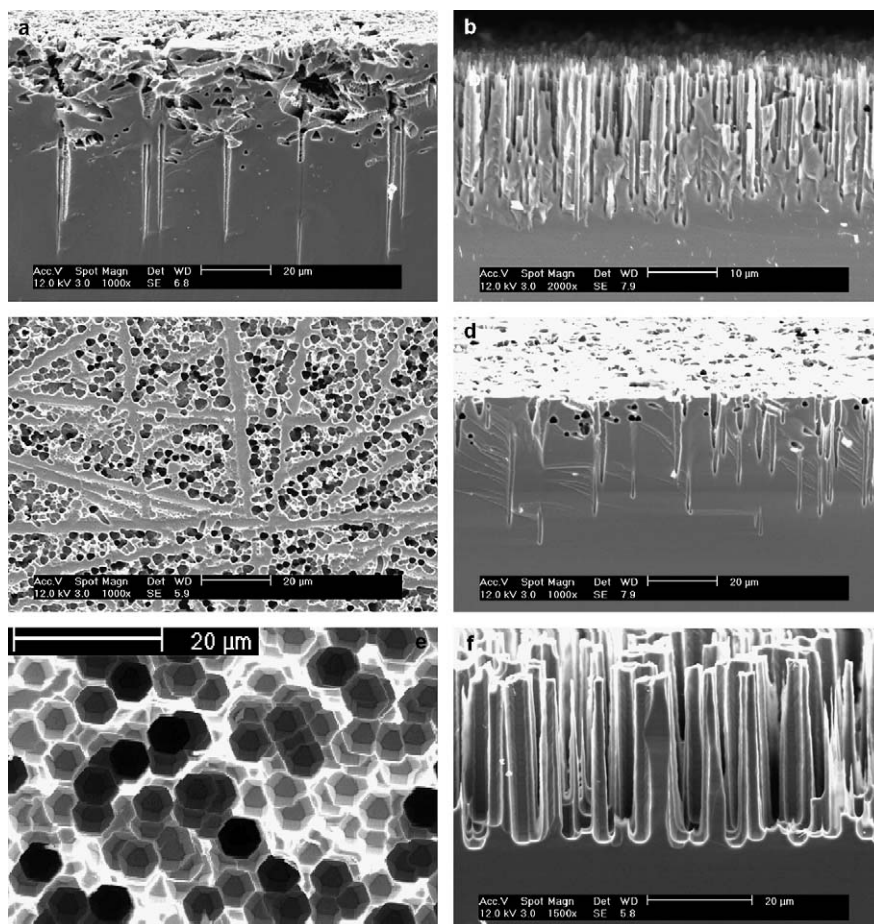


Fig. 24. Pore growth on n-doped {111} sample in HCl/DMSO solution of 5% (a–e), or 7.5% (f), (g); 14 °C, ($n = (10^{15}–10^{16} \text{ cm}^{-3})$). (a) Abraded surface, 10 mA/cm² for 30 min. (b) Rough surface, ramping down 50–5 mA/cm² in 60 min. (c) Smooth surface, after a pulse of 250 mA/cm² for 3 s, 5 mA/cm² for 60 min. (d) Smooth surface, after a pulse of 125 mA/cm² for 6 s, ramping down 25–5 mA/cm² in 60 min. (e) Smooth surface, ramping down 50–5 mA/cm² in 40 min, 0.5 mA/cm² for 100 min. (f) Cross-section of (e).

Accepting that statement for the time being, the lack of chemical reaction equations or standard electrochemical characterization techniques like impedance spectroscopy in this paper may appear incongruous. However, for brevity's sake, we will not duplicate the obvious sets of reaction equations for direct dissolution, oxide formation and oxide dissolution here; in particular because there is at present no good way to differentiate between the plethora of possible reactions. The reason for that is the same as the reason for not presenting impedance spectroscopy data or data from other characterization techniques at this point of the investigations: As long as the pore geometry is very inhomogeneous in space and/or time, all integral characterization methods gather an unqualified mix of data from pore tips, pore walls, surface and non-porous domains (not to mention the area around the O-ring), which can not be deconvoluted in a meaningful way. Easily measured quantities like the valence of the total process or impedance spectra are thus rather meaningless and we will neither present (available) experimental results nor discuss possible implications. We will also not discuss in detail the nucleation and domain formation issues presented in chapter

3.3, but refer to [19,48], where first explanations were attempted that are still valid even in the light of the more recent findings.

Here we will focus on (i) leakage currents, junction breakdown and electropolishing; (ii) surface passivation and pore crystallography; (iii) oxide formation and dissolution.

4.2. Leakage currents, junction breakdown and electropolishing

A n-type semiconductor–electrolyte junction under anodic bias resembles a reversely biased diode up to a point, and this is expressed in its *IV* characteristics including the response to light in all modes (fsi and bsi). Ideally, in the dark, only the junction leakage current is observed, followed by junction breakdown at large potentials. It is helpful to first recall the theoretically predicted leakage currents from the semiconductor side only through (extended and one-dimensional) reversely biased pn-junctions in the Si or Ge case (cf., e.g. [74]), and than to compare it to the experimental observations. We thus neglect possible elec-

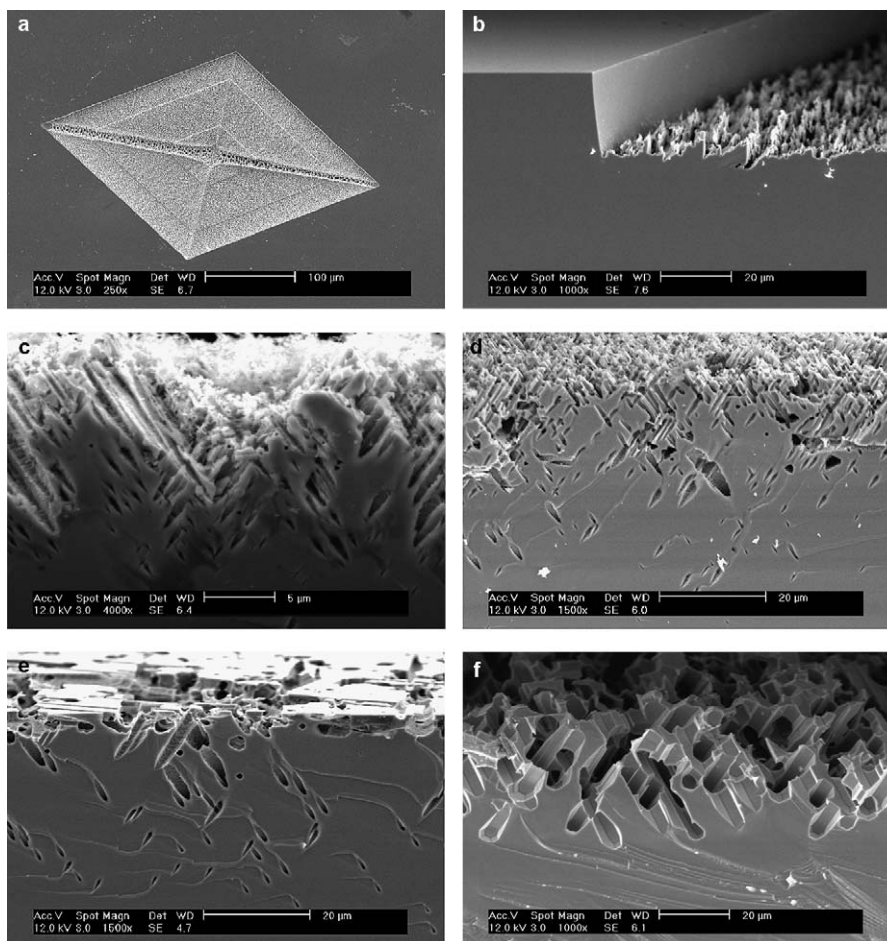


Fig. 25. {110} n-Ge. Low doping (8.5–14.5 Ωcm) in 5% HCl/DMSO electrolyte. All in the dark. (a) Polished surface, ramping current (0–0.5 mA/cm²) in 60 min. (b) Cross-section view of (a). (c) Abraded surface, ramping up current 0–5 mA/cm² in 60 min. (d) Polished surface, ramping down current 50–5 mA/cm² in 60 min. (e) Polished surface, ramping down current 25–2.5 mA/cm² in 60 min. (f) As (e), but additional etching at 0.5 mA/cm² for 1000 min.

tron-injection processes from the electrolyte into the semiconductor. In general, the total (hole) leakage current I_1 from the n-semiconductor part of the junction is given by

$$I_1 = \frac{eLn_i^2}{\tau N_D} + \frac{en_i d_{SCR}}{\tau} \quad (4.1)$$

with e is the elementary charge, L the diffusion length of minority carriers, n_i the intrinsic carrier concentration, N_D the doping concentration, and d_{SCR} the width of space charge region (in the semiconductor). The first term simply includes all the holes generated in the bulk that manage to diffuse to the edge of the space charge region (SCR) and then are (energetically) swept down the reversely polarized junction. The second term (in the standard approximation) adds the current from the minority carriers that are generated in the SCR. This term, however, does not include additional generation at possible interface states that might be present in the junction; the situation for a solid liquid junction thus might be even more involved as described below.

In a first corollary the ratio of the bulk part to the SCR part of the leakage current is

$$\frac{I_1(\text{bulk})}{I_1(\text{SCR})} = \frac{Ln_i}{d_{SCR}N_D} \quad (4.2)$$

This implies that for Si with $n_i(\text{Si}) \approx 10^{10} \text{ cm}^{-3}$ the leakage current results almost exclusively from the SCR and thus shows the (square root) voltage dependence of d_{SCR} , while for Ge with $n_i(\text{Ge}) \approx 2 \times 10^{13} \text{ cm}^{-3}$ the leakage current results almost exclusively from the bulk (and is thus not voltage dependent). Using only the relevant terms one obtains for the ratio of the leakage currents of Si and Ge (assuming that life times are about equal)

$$\frac{I_1(\text{Ge})}{I_1(\text{Si})} = \frac{Ln_i^2(\text{Ge})}{n_i(\text{Si})d_{SCR}N_D(\text{Ge})} \gg 1. \quad (4.3)$$

Since the diffusion length L in electronic grade Si or Ge is always much larger than the SCR width and $n_i(\text{Si})N_D(\text{Ge})$ far smaller than $n_i^2(\text{Ge})$, the leakage current in an extended Ge junction would always be considerably larger than in the Si case. If the leakage current is restricted to the SCR part in Ge, too, because the diode is “thin”, or we are considering a thin region between pore walls, we have for the relation of the leakage currents $I_{1,SCR}$ only from the SCR

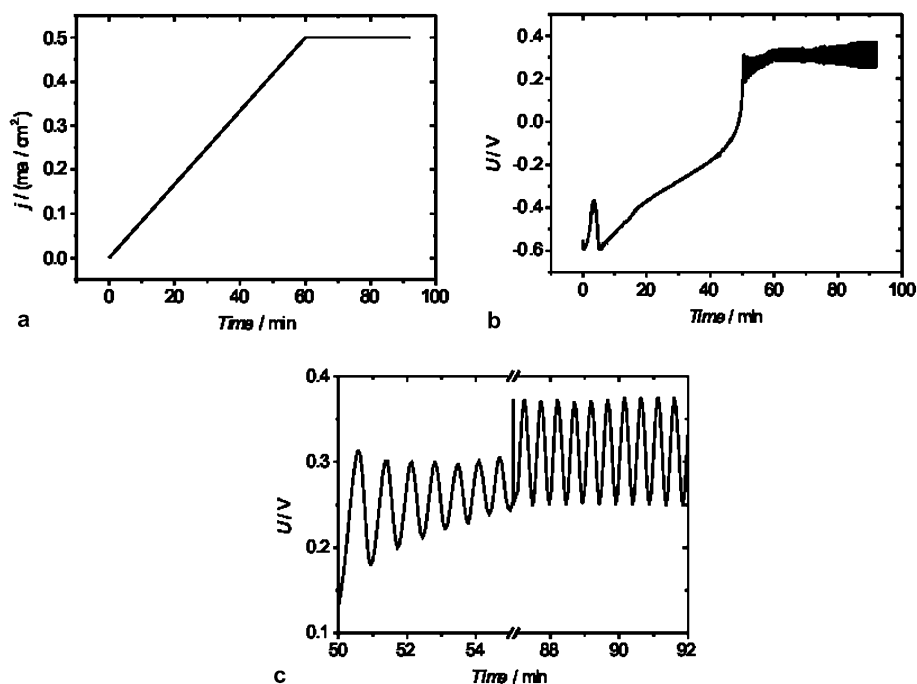


Fig. 26. Potential oscillations obtained with low-doped n-type {110} Ge. Abraded surface. 20 °C, 5% HCl / DMSO electrolyte. (a) Etching current with “up” ramp. (b) Corresponding etching potential. (c) Detail from around the onset and near the end of the voltage oscillations.

$$\frac{I_1(\text{Ge})}{I_{1,\text{SCR}}(\text{Si})} \approx \frac{n_i(\text{Ge})}{n_i(\text{Si})} \approx 2 \times 10^3. \quad (4.4)$$

In other words, while it may appear trivial that Ge draws larger leakage currents than Si, the actual situation is a bit more involved than commonly assumed. Note, for example, that leakage currents from thin junctions are not a direct function of doping (albeit an indirect one via the width of the SCR). Nevertheless, the density of holes available for producing leakage currents is far higher in Ge than in Si (or the common III–V’s). In a real (solid-state) junction some leakage current as expressed in the formulas above would always flow in the reverse direction with a weak dependency on the applied potential. In electrochemical junctions, however, the holes initially flowing into the junction, i.e. to the solid–liquid interface, must find a chemical reaction partner, and that is a major difference to the solid-state case. If the interface is covered with a “passivating” layer, i.e. OH, Cl, or, in the cathodic case involved during the “pulse” experiments or in the membrane switching experiments, with H, finding a reaction partner is difficult. Holes cannot flow out into solution and in consequence the band bending is reduced to levels near flat-band matched to the actual current flow.

Moreover, if a non-conducting layer, e.g. an oxide with a thickness above some tunneling threshold is present at least parts of the time because that is what the current flow produces, local leakage currents turn themselves periodically on and off (cf. the current burst model [34,35,65]), and the average leakage current is smaller than expected from simple “theory”.

All things considered, we must expect now that the leakage currents in Ge, leading to the “electropolishing” effects described before, are far larger than in Si for a variety of reasons: (i) They would already be much larger in simple solid state junction. (ii) Surfaces are less likely to be (very well) passivated by H than in Si since H^+ does not cover Ge surfaces under positive bias and thus have to rely on less efficient passivation with Cl or OH, and (iii) they are less likely to be blocked at least for some of the time because a high-quality oxide is formed by the chemical reaction. While this not only may “explain” some of the general electropolishing observations, it also gives a clear indication that local dissolution of Ge is also quite sensitive to the kind of passivation encountered in a given situation.

In addition, the competition between pore tip current and electropolishing (=leakage current) is far larger than in Si, and this may simply mean that a potential nuclei in the form of a small depression grows laterally so fast that it never has enough time to focus carriers at its tip in order to form a pore. In other words, it is likely and understandable that the critical size of nuclei able to grow macropores under e.g. bsi conditions, for example a lithographically introduced etch pit, must be much larger in Ge than in Si.

In theory, illuminating an (ideal) junction just adds the photo current to the leakage current, and no (non-trivial) differences between Si and Ge are expected. However, proper increase of the current upon illumination can only be expected if the additional holes that reach the interface can be “chemically” processed. In the standard Si case of n-Si-macro (aqu., bsi) conditions this is always the case at the pore tips, but this is not a necessary condition. In

fact, recent experiments with n-Si-macro (org, bsi) pores (triggered to some extent by the Ge results) demonstrate that conditions can be found where illumination does not “register” in the etching current in the expected way [75]. In most of the Ge samples the pore distances were large enough to allow for hole diffusion to the pore walls; the fact that illumination often makes little difference in the pore properties may simply be tied to the complications outlined above. More important, however, seems to be that the breakdown part of the “leakage” current moves to smaller potentials during etching and thus simply overwhelms the photo-induced current.

This leads to the question why breakdown always starts at just a few volts – comparable to the III–V’s, but in stark contrast to Si, where voltages in excess of 100 V are needed in order to induce breakdown in low-doped samples under unassuming standard conditions, and with leakage current in the $\mu\text{A}/\text{cm}^2$ region for all voltages below breakdown. The field strength E_{SCR} in a SCR biased with a voltage U is the basic reason for either tunneling or avalanche breakdown. In the most naïve but sufficient approximation it is given by

$$E_{\text{SCR}} = \left(\frac{2\epsilon\epsilon_0}{eN_{\text{D}}U} \right)^{1/2} \quad (4.5)$$

and thus not much dependent on the semiconductor type for comparable doping. Closer inspection, following e.g. [74] reveals that avalanche breakdown is expected to be the dominant mechanism for breakdown voltages larger than about $4E_{\text{G}}/e$ (E_{G} = bandgap, e = elementary charge), which translates to less than 3 V for Ge. All things considered, avalanche breakdown in Ge happens at considerably lower voltages than in Si (e.g. 8 V instead of 20 V at a doping concentration of about $5 \times 10^{16} \text{ cm}^{-3}$, or 35 V instead of 100 V for about 10^{15} cm^{-3}). But this is still not sufficient to explain why some kind of breakdown is usually found around 5 V independent of doping.

Of course, local defects like dislocations or nano-sized precipitates may locally enhance the field strength to breakdown levels long before global breakdown conditions are reached, as has been demonstrated for III–V’s [76,77] and as can be seen in Fig. 2b. But this effect seems to be on top of the already low breakdown voltage and thus does not explain the peculiar Ge behavior. More generally, all results indicate that hole generation is simply not a problem for electrochemically challenged n-Ge, in pronounced contrast to Si.

The solution to the question may be found in the oxide generation part of the current. In Si any local breakdown at field strengths well below the global breakdown level will rather rapidly seal itself by quickly producing an oxide patch or “oxide bump” that turns off current flow and takes far longer to dissolve than to form. Nuclei for starting local dissolution thus have to be large or otherwise “potent”, and the system tends to have large global breakdown voltages and to form relatively uniform structures

because many pore sites are needed to carry the total current, which at any point in time flows only through a few active sites.

In Ge, the oxide produced seems to be rather impotent as a current stopper; this is illustrated by the fact that large lumps of oxide as shown in Fig. 15 obviously could not stop pore growth. This behavior also accounts naturally, if purely qualitatively at present, for the very basic feature of extremely inhomogeneous pore nucleation under most instances. The domain formation mechanisms as outlined in [19,48] tie in with this, taking both mechanisms (plus some of what will be discussed further on) together, may explain the basic observations made around the many “nucleation improvement” attempts presented.

For the sake of completeness, the mechanism of domain formation will be explained in short as follows: Due to the fact that the current flows also through the pore walls, each breakdown-nucleated pore will be a large current sink. Thus, due to ohmic and diffusion losses, the voltage around each pore will be reduced as illustrated in Fig. 27, i.e. the etching conditions will tend to move somewhere between regions II and I thus favoring pore formation. New pores thus nucleate preferentially around old pores, leading to the pore domains as shown in Fig. 3. This is a self-amplifying process since the additional pores further increase the local current, and so on.

4.3. Surface passivation concerns

For Si in the cathodic as well as in the anodic pore formation regime, H is the surface passivation species. In contrast, the surface passivation species and its kinetics on a $\{hkl\}$ Ge surface depend strongly on the chosen electrolyte and the applied voltage. In an aqueous solution of HClO_4 or H_2SO_4 a change from $-\text{H}$ to $-\text{OH}$ passivation has been confirmed by FT-IR at a potential of -0.2 V (vs. SCE), and there are hints that in the anodic regime $-\text{OH}$ is the thermodynamically stable passivation species [3,4,78–80]. In HF containing systems a $-\text{H}$ terminated interface has been confirmed by FT-IR [23], which could be replaced after thermal oxidation at $600 \text{ }^\circ\text{C}$ by Ge-O-Ge and $-\text{OH}$

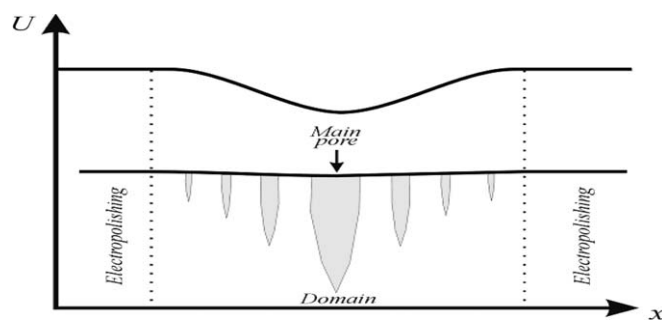


Fig. 27. Model for domain formation. The voltage across the semiconductor/electrolyte junction is decreased around the main pore, leading to a preferential nucleation of new pores. Outside this region electropolishing dominates.

bonds. The group of Buriak found -H passivation as well [9,81], but pointed out that a -H terminated Ge surface is kinetically not stable (Ge-H, 322 kJ/mol; Ge-F, 485 kJ/mol; Ge-Cl, 431 kJ/mol). Other papers show that the Ge surface can be -Cl passivated as well, e.g. the immersion of an oxidized (111) surface into a HCl solution leads to a -Cl terminated surface as a perfect monolayer [82–85]. It is safe to assume that the enthalpies involved as well as the kinetics (i.e. the time needed for coverage of a “fresh” surface) is $\{hkl\}$ dependent; which is most likely also true for the oxide formation parameters.

The overwhelmingly rich diversity with respect to the crystallography expressed in Ge pore tips, pore walls and all other surfaces could be well understood by the far more diversified passivation chemistry and kinetics compared to Si. There are several parts to this statement. First, the question is which chemical species would cover a given convoluted (=porous) Ge surface under the prevailing conditions in equilibrium (e.g. after switching off the current). Second, it needs to be assessed how long this process would take if the surface was covered with something else before. Third, the electrical property of the surface layer, i.e. its “passivation” properties relative to (leakage) current flow, needs to be known. Fourth, all of the above must be considered as a function of crystallography and temperature (and electrolyte composition, pH, etc.). In Si, the first three points are simple: In a very rough approximation, the surface will always be covered with -H as soon as the oxide is dissolved and this efficiently impedes (leakage) current flow. The dependence of this -H passivation on the crystallography (and temperature) is the only major factor that must be considered; nevertheless it is sufficient to introduce quite a wealth of features in Si (e.g. $\langle 113 \rangle$ pores). Modifying the H^+ passivation somewhat by the addition of surfactants introduces more features and complications [86,87].

It should be added however that not only the passivation may introduce anisotropies and thus lead to crystallographic pores with or without prismatic shapes, but also the oxide formation and the avalanche breakdown. The former effect exists for thermal oxidation of Si; but little seems to be known about the anodic oxidation of Si (cf. [16]) and presumably even less about the other semiconductors. The latter effect can be rather large breakdown voltages may differ by more than a factor of 2 for e.g., $\{111\}$ vs. $\{110\}$ in GaAs, cf. [74], but to the best of our knowledge has not yet been invoked in pore formation. In the standard Si n-macro (aqu, bsi) case it is not needed, anyway, but in pores associated with breakdown like in Ge or the III-V's, it may play a role.

4.4. Oxide formation and dissolution

GeO_2 is not a “good” oxide if compared to SiO_2 : It is rather unstable and dissolves in almost everything, and it cannot sustain a large field strength. Nevertheless, it can build up in a pore; an effect never observed with other porous semiconductors. There might be two basic reasons for

this: (i) More degrees of freedom concerning (current driven) oxide formation and (chemically driven) dissolution in Ge may enable ratios of formation rates/dissolution rates not found in Si, and (ii) local oxide formation is not able to suppress Ge dissolution completely, as is most likely the case in Si. Some first experiments with GeO_2 saturated electrolytes along the first item did not (yet) produce conclusive results, but the sheer presence of oxide filled pores does confirm that dissolution below an oxide is indeed possible.

It may be speculated that most, if not all “large” pores presented in most of the figures before are somehow connected to this Ge particularity, and that “true” or “SCR” macropores, with geometries determined mostly by SCR width and thus doping, are only found in competition to this “oxide pore” growth mechanisms. There are some indications for this, Fig. 28 shows an example. One might speculate that only the small $\langle 111 \rangle$ oriented pores are SCR pores, whereas the large $\langle 100 \rangle$ pores are of the “oxide” type. However, while this may provide a certain direction for further studies, it would be premature to be belaboring this point much more at present.

4.5. Final remarks

In the light of what has been discussed so far, a few more or less speculative interpretations of some of the results will be made in a very short form:

4.5.1. Aqueous electrolyte

At low HCl concentration (<2%) pores grow slowly into the depth (with strong lateral growing components). In this region probably the oxide dissolution rate is the relevant reaction controlling kinetics. Ge surfaces start to be covered with oxide, but pore growth is still (in contrast to Si) because to their inferior quality of the “leaky” oxide.

In an intermediate range of HCl concentration (4–5%) OH passivation is dominant, leading to well-expressed $\{110\}$ walls. This is the most stable plane and here we have the optimal conditions for pore growth in combination with methods for homogeneous nucleation.

For higher HCl concentration (>5%) the Cl-passivation becomes decisive. The competition between Cl- and OH-passivation allows for additional pore growth directions and pore walls, but hinders the formation of “nice” deep pores.

4.5.2. Organic electrolyte

In organic (=almost water-free) electrolytes no or only rather weak OH-passivation occurs. Therefore no good deep pores are found. Only Cl passivation exists, leading to comparable pore structures as in the case of high Cl concentration in aqueous electrolytes, but without effects related to the competition of two different passivation chemistries. At high current densities pores are found which do not grow very deep, and which do not show $\{110\}$ walls. At low current densities surface structures

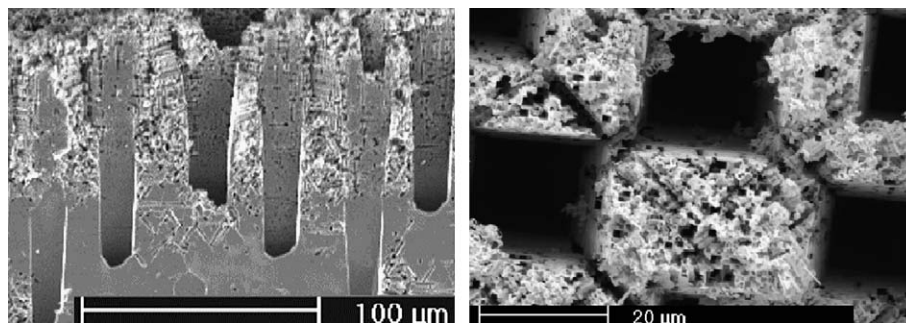


Fig. 28. Cross-section and top view of concurrently etched “oxide pores” and “SCR pores”. Two-step etching of n-type Ge in the dark, $0.04 \Omega\text{cm}$, (100), rough surface, $T = 24^\circ\text{C}$. First step 5.5% HCl aqueous electrolyte, ramp potential from 0 to 20 mA/cm² in 60 min, then 20 mA/cm² 30 min. Second step 2.7% HCl aqueous electrolyte, 900 mA 0.6 s, ramp potential from -0.2 to 1.5 V in 300 min, then 1.5 V, 600 min n-type in the dark.

are formed with nice crystallographic “pore” walls other than {110}.

The essential advantage of organic electrolyte in Si (less oxide formation, but the dominant H passivation is still possible) thus is not so important for Ge. Here the oxide is “weak” and the OH passivation (most favorable for Ge pore formation) is replaced by Cl passivation. What still allows pores, in particular in p-type Ge, results from different surface passivation kinetics in comparison to aqueous electrolytes.

Acknowledgements

The authors thank Prof. Eugen Haller, who supplied them with the first Ge samples allowing us to start this work; Dr. Sergiu Langa, who did the very first successful experiments; Ms. Le Jiang who produced a series of porous Ge samples, and Mr. Stefan Frey who contributed by suggestions and many fruitful discussions. The “Deutsche Forschungsgemeinschaft” (DFG) supported this work under Grant No. FO 258/7-1.

References

- [1] J. Bardeen, W.H. Brattain, *Phys. Rev.* 74 (1948) 230.
- [2] D.R. Turner, in: P.J. Holmes (Ed.), *The Electrochemistry of Semiconductors*, vol. 155, Academic Press, New York, 1962.
- [3] H. Gerischer, A. Mauerer, W. Windt, *Surf. Sci.* 4 (1966) 431.
- [4] R. Memming, G. Neumann, *J. Electroanal. Chem.* 21 (1969) 295.
- [5] P. Singer, *Semiconductor Int.* (2004) 1.
- [6] L.K. van Vugt, A.F. van Driel, R.W. Tjerkstra, L. Bechger, D. Vanmaekelbergh, J.J. Kelly, *Chem. Commun.* 62 (2002) 2054.
- [7] K. Busch, S. Lölkes, R.B. Wehrspohn, H. Föll (Eds.), *Photonic Crystals: Advances in Design, Fabrication, and Characterization*, Wiley-VCH, Weinheim, 2004.
- [8] J.-N. Chazalviel, A. Belaidi, M. Safi, F. Maroun, B.H. Erne, F. Ozanam, *Electrochem. Acta* 45 (2000) 3205.
- [9] K. Choi, J.M. Buriak, *Langmuir* 16 (2000) 7737.
- [10] J.M. Buriak, *Chem. Rev.* 102 (5) (2002) 1271.
- [11] H. Föll, S. Langa, J. Carstensen, M. Christophersen, I.M. Tiginyanu, *Adv. Mater.* 25 (2003) 183.
- [12] A.G. Cullis, L.T. Canham, P.D.J. Calcott, *Appl. Phys. Rev.* 82 (3) (1997) 909.
- [13] J.-N. Chazalviel, R. Wehrspohn, F. Ozanam, *Mater. Sci. Eng. B* 69–70 (2000) 1.
- [14] H. Föll, M. Christophersen, J. Carstensen, G. Hasse, *Mater. Sci. Eng. R* 39 (4) (2002) 93.
- [15] V. Lehmann, *Electrochemistry of Silicon*, Wiley-VCH, Weinheim, 2002.
- [16] X.G. Zhang, *Electrochemistry of Silicon and its Oxide*, Kluwer Academic/Plenum Publishers, New York, 2001.
- [17] L.T. Canham, V.P. Parkhutik, *Phys. Stat. Sol. (a)* 182(1) (2000).
- [18] L.T. Canham, A. Nassiopoulou, V. Parkhutik, *Phys. Stat. Sol. (a)* 197 (2003).
- [19] S. Langa, M. Christophersen, J. Carstensen, I.M. Tiginyanu, H. Föll, *Phys. Stat. Sol. (a)* 195 (2003) R4.
- [20] M. Matsumura, S.R. Morrison, *J. Electroanal. Chem.* 147 (1983) 157.
- [21] S. Cattarin, M. Musiani, *J. Electroanal. Chem.* 572 (2004) 257.
- [22] M. Sendova-Vassileva, N. Tzenov, D. Dimova-Malinovska, M. Rosenbauer, M. Stutzmann, K.V. Josepovits, *Thin Solid Films* 255 (1994) 282.
- [23] S. Miyazaki, K. Sakamoto, K. Shiba, M. Hirose, *Thin Solid Films* 255 (1995) 99.
- [24] S. Bayliss, Q. Zhang, P. Harris, *Appl. Surf. Sci.* 102 (1996) 390.
- [25] S.S. Chang, R.E. Hummel, *J. Luminesc.* 86 (2000) 33.
- [26] G. Kartopu, V.A. Karavanskii, U. Serincan, R. Turan, R.E. Hummel, Y. Ekinici, A. Gunnes, T.G. Finstad, *Phys. Stat. Sol. A* 202 (8) (2005) 1472.
- [27] G. Flamand, J. Poortmans, K. Dessenin, *Phys. Stat. Sol. (c)* 2 (9) (2005) 3243.
- [28] C.S. Solanki, R.R. Bilyalov, J. Poortmans, J.-P. Celis, J. Nijs, *Phys. Stat. Sol. (a)* 197 (2003) 507.
- [29] S. Langa, J. Carstensen, M. Christophersen, H. Föll, I.M. Tiginyanu, *Appl. Phys. Lett.* 78 (2001) 1074.
- [30] E.K. Propst, P.A. Kohl, *J. Electrochem. Soc.* 141 (1994) 1006.
- [31] E.A. Ponomarev, C. Levy-Clement, *Electrochem. Solid-State Lett.* 1 (1) (1998) 42.
- [32] E.A. Ponomarev, C. Levy-Clement, *J. Porous Mater.* 7 (2000) 51.
- [33] M. Christophersen, J. Carstensen, K. Voigt, H. Föll, *Phys. Stat. Sol. (a)* 197 (1) (2003) 34.
- [34] H. Föll, J. Carstensen, M. Christophersen, G. Hasse, *Phys. Stat. Sol. (a)* 182 (1) (2000) 7.
- [35] J. Carstensen, M. Christophersen, G. Hasse, H. Föll, *Phys. Stat. Sol. (a)* 182 (1) (2000) 63.
- [36] P.J. Holmes (Ed.), *The Electrochemistry of Semiconductor*, Academic Press, New York, 1962.
- [37] S. Frey, M. Kemell, J. Carstensen, S. Langa, H. Föll, *Phys. Stat. Sol. (a)* 202 (2005) 1369.
- [38] S. Langa, S. Frey, J. Carstensen, H. Föll, I.M. Tiginyanu, M. Hermann, G. Böttger, *Electrochem. Solid-State Lett.* 8 (2005) C30.
- [39] S. Langa, J. Carstensen, I.M. Tiginyanu, M. Christophersen, H. Föll, *Electrochem. Solid State Lett.* 4 (2001) 50.
- [40] H. Föll, J. Carstensen, S. Langa, M. Christophersen, I.M. Tiginyanu, *Invited paper to PSST-2002, Phys. Stat. Sol. (a)* 197(1/2) (2003).

- [41] H. Föll, S. Langa, J. Carstensen, I.M. Tiginyanu, M. Christophersen, K. Dichtel, in: R.B. Wehrspohn, S. Noda, C. Soukoulis, R. März (Eds.), MRS Proceedings Spring Meeting: Materials and Devices for Optoelectronics and Microphotonics L6.4, 2002.
- [42] V. Lehmann, H. Föll, J. Electrochem. Soc. 137 (1990) 653.
- [43] M. Christophersen, J. Carstensen, S. Rönnebeck, C. Jäger, W. Jäger, H. Föll, J. Electrochem. Soc. 148 (2001) E267.
- [44] S. Langa, J. Carstensen, I.M. Tiginyanu, M. Christophersen, H. Föll, Electrochem. Solid State Lett. 5 (2002) 14.
- [45] S. Langa, J. Carstensen, M. Christophersen, I.M. Tiginyanu, H. Föll, Phys. Stat. Sol. (a) 197 (1/2) (2003).
- [46] S. Langa, J. Carstensen, I.M. Tiginyanu, M. Christophersen, H. Föll, in: R.B. Wehrspohn (Ed.), Ordered Porous Nanostructures and Applications, 2005, p. 57.
- [47] J.H. Erne, D. Vanmaekelbergh, J.J. Kelly, J. Electrochem. Soc. 143 (1996) 305.
- [48] S. Langa, J. Carstensen, M. Christophersen, K. Steen, S. Frey, I.M. Tiginyanu, H. Föll, J. Electrochem. Soc. 152 (2005) C525.
- [49] J. Wloka, K. Mueller, P. Schmuki, Electrochem. Solid-State Lett. 8 (12) (2005) B72.
- [50] L.T. Canham, A. Nassiopoulou, V. Parkhutik, Phys. Stat. Sol. (a) 202(8) (2005).
- [51] ET&TE Etch and Technology GmbH. Available from: <<http://www.et-te.com>>.
- [52] S. Langa, M. Christophersen, J. Carstensen, I.M. Tiginyanu, H. Föll, Phys. Stat. Sol. (a) 197 (1/2) (2003).
- [53] F. Mugele, A. Klingner, J. Buehrle, D. Steinhauser, S. Herminghaus, J. Phys.: Condens. Matter 17 (2005) S559.
- [54] M. Christophersen, J. Carstensen, H. Föll, Phys. Stat. Sol. (a) 182 (1) (2000) 103.
- [55] S. Rönnebeck, J. Carstensen, S. Ottow, H. Föll, Electrochem. Solid State Lett. 2 (1999) 126.
- [56] S. Rönnebeck, S. Ottow, J. Carstensen, H. Föll, J. Porous Mater. 7 (2000) 353.
- [57] J.S. Shor, L. Bemis, A.D. Kurtz, I. Grimberg, B.Z. Weiss, M.F. MacMillan, W.J. Choyke, J. Appl. Phys. 76 (7) (1994) 4045.
- [58] C. Fang, S. Langa, L. Jiang, J. Carstensen, E. Foca, H. Föll, Electrochemical pore etching in Germanium, 2005, p. 3.8.
- [59] J. Diener, N. Künzner, D. Kovalev, E. Gross, V.Y. Timoshenko, G. Polisski, F. Koch, Appl. Phys. Lett. 78 (2001) 3887.
- [60] V. Kochergin, Omnidirectional Optical Filters, Kluwer Academic Publishers, Boston, 2003.
- [61] V. Kochergin, M. Christophersen, H. Föll, Appl. Phys. B 79 (6) (2004) 731.
- [62] D.R. Turner, J. Electrochem. Soc. 105 (1958) 402.
- [63] J.-N. Chazalviel, F. Ozanam, M. Etman, F. Paolucci, L.M. Peter, J. Stumper, J. Electroanal. Chem. 327 (1992) 343.
- [64] V. Lehmann, J. Electrochem. Soc. 143 (1996) 1313.
- [65] J. Carstensen, R. Prange, G.S. Popkirov, H. Föll, Appl. Phys. A 67 (1998) 459.
- [66] M. Christophersen, S. Langa, J. Carstensen, P.M. Fauchet, H. Föll, in MRS Proceedings Spring Meeting: Invited Paper, 2003.
- [67] J. Grzanna, H. Jungblut, H.J. Lewerenz, J. Electroanal. Chem. 486 (2000) 190.
- [68] E. Harvey, D.N. Buckley, S.N.G. Chu, Electrochem. Solid State Lett. 5 (4) (2002) G22.
- [69] J. Wloka, D.J. Lockwood, P. Schmuki, Chem. Phys. Lett. 414 (2005) 47.
- [70] M.I.J. Beale, J.D. Benjamin, M.J. Uren, N.G. Chew, A.G. Cullis, J. Cryst. Growth 73 (1985) 622.
- [71] P.C. Searson, J.M. Macaulay, S.M. Prokes, J. Electrochem. Soc. 139 (1992) 3373.
- [72] R.L. Smith, S.D. Collins, J. Appl. Phys. 71 (1992) R1.
- [73] G.C. John, V.A. Singh, Phys. Rep. 263 (1995) 93.
- [74] S.M. Sze, Physics of Semiconductor Devices, Wiley, New York, 1981.
- [75] to be published.
- [76] P. Schmuki, L.E. Erikson, D.J. Lockwood, B.F. Mason, J.W. Fraser, G. Champion, H.J. Labbe, J. Electrochem. Soc. 146 (1999) 735.
- [77] P. Schmuki, L. Santinacci, T. Dienizian, D.J. Lockwood, Phys. Stat. Sol. (a) 182 (1) (2003).
- [78] J.-N. Chazalviel, F. Maroun, F. Ozanam, J. Electrochem. Soc. 152 (2) (2004) E51.
- [79] F. Maroun, F. Ozanam, J.-N. Chazalviel, J. Phys. Chem. B 103 (1999) 5280.
- [80] F. Maroun, J.-N. Chazalviel, F. Ozanam, D. Lincot, J. Electroanal. Chem. 549 (2003) 161.
- [81] H.C. Choi, J.M. Buriak, Chem. Commun. 17 (2000) 1669.
- [82] Z.H. Lu, App. Phys. Lett. 68 (4) (1996) 520.
- [83] G.W. Cullen, J.A. Amick, D. Gerlich, J. Electrochem. Soc. 109 (1962) 124.
- [84] Z.H. Lu, T. Tylliszczak, A.P. Hitchcock, M.W.C. Dharma-Wardana, Surf. Sci. 442 (1999) L948.
- [85] S. Cao, J.-C. Tan, S.-L. Shen, J. Phys.: Condens. Matter 15 (2003) 5261.
- [86] K.J. Chao, S.C. Kao, C.M. Yang, M.S. Hseu, T.G. Tsai, Electrochem. Solid State Lett. 3 (2000) 489.
- [87] S. Schweizer, R.B. Wehrspohn, J. Schilling, in: 203rd meeting of the Electrochemical Society, Paris, 2003 (Abstract 2747).